Direct observation of tunneling reactions by matrix isolation spectroscopy

Cláudio M. Nunes[a], Igor Reva[a] and Rui Fausto[a,b]

[a] CQC, Department of Chemistry, University of Coimbra, 3004-535 Coimbra.

[b] Department of Chemistry, King Fahd University of Petroleum and Minerals, 31261 Dhahran, Saudi Arabia.

Author emails: cmnunes@qui.uc.pt; reva@qui.uc.pt; rfausto@ci.uc.pt

ABSTRACT

Direct observation of tunneling reactions of organic molecules under low temperature matrix isolation conditions using infrared spectroscopy as probing technique is described. The considered types of tunneling-driven reactions include conformational rearrangements, as well as bond-forming/bond-breaking processes that take place either by hydrogen atom tunneling or heavy atom tunneling. The advantages and peculiarities of the matrix isolation method to allow for the direct observation of the tunneling reactions are highlighted. Methods of *in situ* preparation of the reactants using photochemical approaches involving vibrational or electronic excitation are presented. Overview of the most recent publications describing observations of tunneling isomerizations is included.

X.1 Introduction

The theoretical foundations for nuclei and electron tunneling were put forward by Hund,[1] Wigner,[2] Bell,[3] and others,[4,5] following the establishment of quantum mechanics. A more generalized treatment of tunneling in chemistry appeared almost half-century afterwards in the seminal Bell's monography *"The Tunnel Effect in Chemistry"*.[6,7] Indeed, as addressed in several other chapters of this book, theoretical methodologies to treat quantum mechanical tunneling (QMT) in chemical reactions are still being developed nowadays. In this chapter, QMT in chemistry will be addressed from a more experimental perspective, taking advantage of the conditions typical of a matrix isolation experiment, which allow for direct observation of tunneling driven processes by steady state spectroscopic methods.

A simple and common way to portrait tunneling, although not particularly accurate,[8] is to consider it as a phenomenon that arises from the wave-particle duality. If in a chemical reaction the moving distance of a nucleus is comparable to its de Broglie wavelength, then there is a non-negligible probability of finding the nucleus on the other side of the reaction barrier, even if the system does not possess enough thermal energy to surmount the barrier. It means that nuclei are able to penetrate through reaction barriers. Of course, such unexpected behaviour is framed on a classic perspective, in which all atoms involved in a chemical transformation are assumed to behave as hard spheres.

According to the classic transition state theory (TST), reactants must acquire enough energy to overcome a barrier in order to give rise to products.[9–11] Statistically, as temperature increases more molecules will have enough energy to traverse the barrier, so that the reaction rate typically increases proportionally. Such temperature

dependence of reaction rates was empirically established by Arrhenius in his well-known equation [Eq. (X.1)], long before the development of the TST.[11,12]

$$k = Ae^{\left(-\frac{E_a}{RT}\right)} \qquad \text{(X.1)}$$

In Eq. (X.1), A is a pre-exponential constant, E_a the activation energy (J mol^{-1}), R the universal gas constant (8.314 J mol^{-1} K^{-1}), and T (K) is the absolute temperature.

However, deviations from the Arrhenius typical behaviour can take place if tunneling occurs simultaneously with the classic passage over the barrier. In these cases, the QMT contribution to the reaction rate can be incorporated using a tunneling correction factor Q in the kinetic models, as it is, for instance, shown in Eq. (X.2).[6,11,13]

$$k = QAe^{\left(-\frac{Ea}{RT}\right)} \qquad \text{(X.2)}$$

The tunneling correction factor Q takes into account the tunneling permeability through the barrier, which depends on the mass of the tunneling particle, as well as on the barrier height and width.[6,13]

The existence of QMT contribution to a chemical reaction is typically detected indirectly by the observation of nonlinear Arrhenius plots or abnormal kinetic isotope effects.[14–18] The temperature dependence of k in Eq. (X.1) is given by the exponential factor, $\exp(-E_a/RT)$. Consequently, a plot of $\ln(k)$ against $1/T$ results in a straight line (see Figure X.1). Its slope is $-E_a/R$. For historic reasons, such plots are referred to as Arrhenius plots. On the other hand, contrary to the classical over-the-barrier thermal process, tunneling rates are approximately independent of the temperature. For a low enough temperature, when the system is in its ground

vibrational state, the overall reaction rate is dominated by tunneling and, consequently, temperature independent (see Figure X.1).

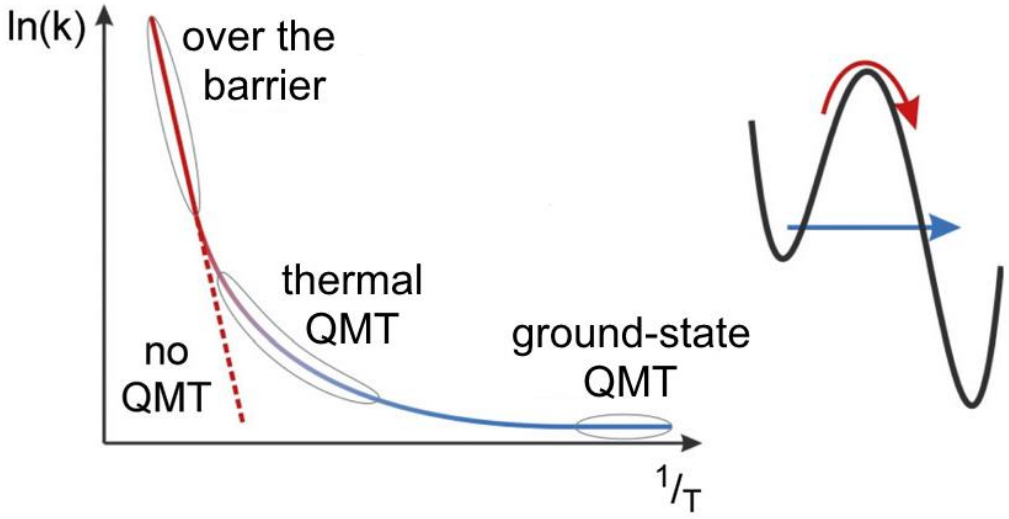

Figure X.1. Logarithm of the rate constant plotted *versus* the inverse temperature (Arrhenius plot). The classical (thermal) over-the-barrier reaction results in a straight line. The rate becomes constant at low temperature when ground-state quantum-mechanical tunneling (QMT) dominates. Adapted from Ref. 15 with permission from The Royal Society of Chemistry.

Working at low temperatures is in fact a very convenient way to search for evidence of tunneling in chemical reactions. At cryogenic temperatures (*e.g.*, 3−10 K), thermally activated rates become negligible for systems having barriers as low as ~4 kJ mol^{-1} (~1 kcal mol^{-1}) so the occurrence of a chemical transformations can only be due to a "pure" tunneling reaction.[14–18] If such tunneling transformation span from seconds to days, they can be directly observed and monitored using stationary state spectroscopy methods. Indeed, particularly during the last decade, direct spectroscopic evidence of a variety of tunneling-driven reactions has been reported using the low temperature matrix isolation technique coupled to infrared

spectroscopy. These observations have contributed significantly to better understanding of QMT and its role in chemistry.[19]

In this chapter, we will address some representative cases of tunneling-driven chemical processes, from conformational isomerizations to H-atom and heavy-atom bond-breaking/bond-forming reactions occurring in organic molecules under matrix isolation conditions. Examples of tunneling reactions at cryogenic temperatures taking place in other than matrix isolation conditions are outside the scope of this chapter.

X.2 Description of simple mathematic models for tunneling computations

The present chapter is not concerned with the theory of tunneling. There are several recent reviews on the topic.[18,20-22] Here we shall remind that any occurrence of a tunneling reaction must always face a barrier to overcome. This section will present simple formulas for the probabilities of tunneling through two barriers of different shapes.

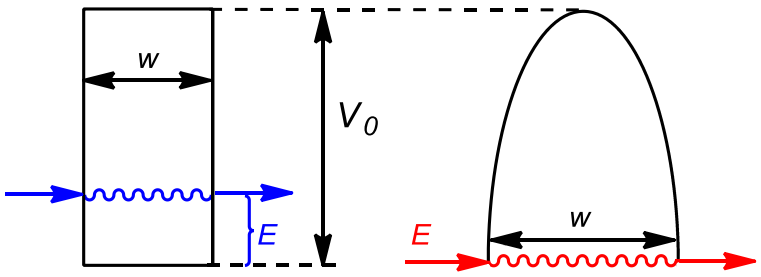

Figure X.2. Left. Tunneling through a rectangular barrier of width *w*, at an energy V_0-E below the top of the barrier. Right. Tunneling through a parabolic barrier of width *w*, at an energy V_0-E below the top of the barrier.

In the recent review,[22] Borden presents the formula for the energy-dependent probability *P(E)*, of a particle with mass *m*, tunneling through a rectangular barrier of width *w* that is V_0-*E* higher than the energy of the particle (see Figure X.2, left):

$$P(E) = e^{-4\pi w\sqrt{2m(V_0-E)}/h} \qquad \text{(X.3)}.$$

A more realistic barrier shape is that of the inverted parabola (as in Figure X.2, right). The approximate solutions for the equations describing the tunneling of a particle through a parabolic barrier were independently devised by Wentzel, Kramers, and Brillouin in 1926.[23-25] As it is noted by Borden,[22] *"what has become known as the WKB approximate solution*[23-25] *to the calculation of the probability of tunneling through a parabolic barrier should really be known as the JWKB approximate solution",*[22] because *"earlier Jeffreys*[26] *had published the mathematics necessary to obtain approximate solutions to differential equations of this type"*.[22] The probability *P(E)* of tunneling through a parabolic barrier in the JWKB approximation can be written as:

$$P(E) = e^{-\pi^2 w\sqrt{2m(V_0-E)}/h} \qquad \text{(X.4)},$$

where a particle with mass *m* tunnels through a barrier with height V_0 and width *w*, (V_0−*E*) is the energy deficiency of the particle with respect to the top of the barrier (Figure X.2, right), and *h* is the Planck's constant.

The exponential Eqs. (X.3) and (X.4) are very similar; they only differ by a factor of π/4, related to the different shapes. Tunneling through a parabolic barrier is more probable than through a rectangular barrier with the same energy deficiency (V_0−*E*), and barrier width, *w*. Both equations show that the probability of tunneling decreases exponentially with the barrier width, *w*, times the square root of the particle mass, *m*, times the square root of the energy deficiency, (V_0−*E*). Therefore, the probability of

tunneling is much more sensitive to the width (*w*) of the barrier than it is to the height (*i.e.*, the energy deficiency), or to the tunneling mass.

The contemporary methods of quantum chemistry allow for a detailed characterization of potential energy surfaces (PES). These include not only information about stationary points (local minima and transition states), but also may provide information about the shape of potential energy barriers. In practice, the characterization of the reaction path starts with optimization of a transition state whose initial geometry and the initial force constants are calculated analytically. The intrinsic reaction path is then followed in both directions from that point, for a monomeric molecule in vacuum, typically with the Gaussian 09 set of programs.[27] Note that the intrinsic reaction coordinate (IRC) may be computed either in the default mass-weighted coordinates (expressed in the [amu$^{-1/2}$ Bohr] units), or in non-mass-weighted (Cartesian) coordinates, by using the "IRC=Cartesian" option, expressed in units of Bohr. The latter option was used in this work in order to obtain the barrier width in units of length (Bohr) for tunneling reactions in systems with OH or SH groups that involve a torsional reaction coordinate (flip by 180°).

An example of such a computed reaction path is presented in Figure X.3 for the OH torsion connecting two amino-hydroxy conformers of cytosine. This allows for a direct estimation of the barrier width from the computed IRC scan at different relative energies. For example, the distance between the ends of the scan, *i.e.* at the points where the IRC scan converges to the minima, can be considered as the upper limit for the width of the barrier. For the current system this limit is *ca.* 2.54 Å (from −2.4 to +2.4 Bohr, Figure X.3). Accounting for the zero-point vibrational energy (ZPE) will reduce the barrier width. In the case of tunneling from **AH2** to **AH1**, *via* the intramolecular OH torsion, the vibrational mode along the intrinsic reaction

coordinate is τ(OH), with a computed frequency of 541 cm^{-1}. Accounting for the ZPE energy of this vibration (3.2 kJ mol^{-1}), the ZPE-corrected barrier width becomes *ca.* 1.77 Å (from −1.72 to +1.62 Bohr, Figure X.3). Above the ZPE level, the shape of the barrier is very close to the inverted parabola, and the WKB approximation can be used for a rough estimation of the probability of tunneling.

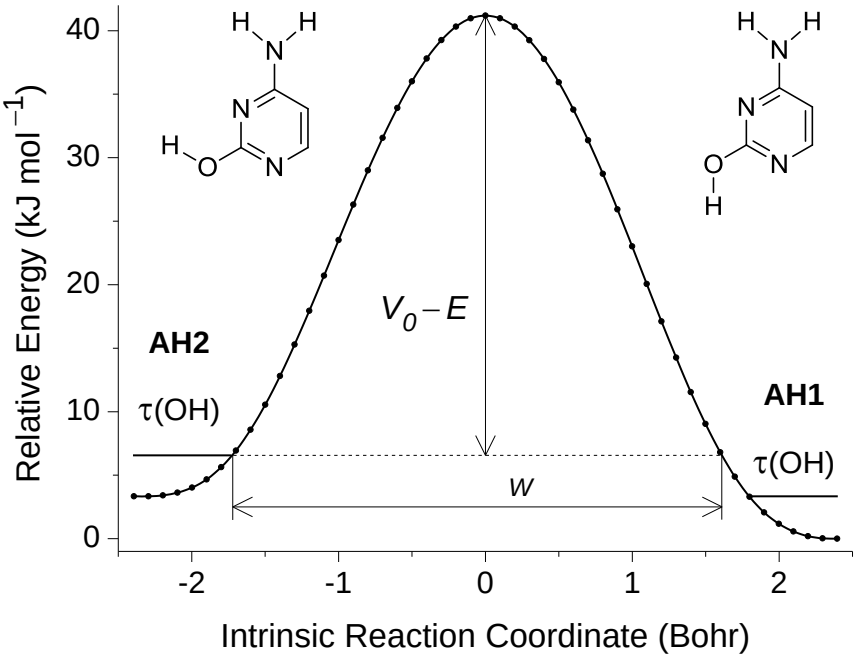

Figure X.3. Intrinsic reaction coordinate (IRC) profile for rearrangement from **AH2** to **AH1** conformer of cytosine, via intramolecular torsion of the OH-group, computed at the B3LYP/6-31++G(d,p) level in Cartesian (non-mass-weighted) coordinates. The vertical arrow (V_0-E = 34.6 kJ mol^{-1}) designates the calculated ZPE-corrected energy of the transition state relative to the reactant (**AH2**, left). The horizontal arrow designates the width (w = 3.34 Bohr) of the barrier at the ZPE level of the reactant.

Using the calculated barrier height of 34.6 kJ mol^{-1} and 1.77 Å width at the ZPE level, the probability of tunneling (transmission coefficient) of **AH2** can be estimated

(using Eq. (X.4)) as 1.6×10^{-16}. The tunneling rate is a product of the transmission coefficient and the frequency of attempts. In this model calculation, assuming that the light H atom of the hydroxyl group of **AH2** conformer is vibrating at the OH torsional frequency of ~541 cm^{-1} (B3LYP/6-31++G(d,p) computed value), it results in a tunneling rate of 2.6×10^{-3} s^{-1}, *i.e.* a half-life time of 4.4 min, which is shorter than the experimentally observed lifetime of several hours. We shall note here that tunneling lifetimes are known to be extremely sensitive to the barrier height and width.[28] Considering that the barrier shape for a molecule in a cryogenic matrix differs from that calculated for a molecule in vacuum,[29] we may carry out another rough estimate of the tunneling lifetime, introducing a ±15% tolerance interval for the barrier width. With a barrier 2.03 Å wide (*i.e.*, increased by 15%), and all other parameters equal, the tunneling half-life time of the **AH2** form of cytosine is then estimated to be 17.3 hours, similar to that obtained in the experiment.[30] With a barrier 1.50 Å wide (*i.e.*, reduced by 15%), and all other parameters equal, the estimated tunneling half-life becomes only 1.1 seconds. This example shows how much sensitive is the probability of tunneling to the width (*w*) of the barrier.

In the above example, we have implemented the WKB approximation, which allows defining a minimum-energy tunneling path by following the intrinsic reaction coordinate. To apply the semi-classical approximation to multidimensional systems, many methods have been developed over the years; they can be classified according to the choice of the tunneling path. The most likely tunneling path differs from the minimum-energy path. A classical particle would take the path which requires least energy to proceed from reactant to the product (only the height of the energy barrier is relevant). Such method is called a zero-curvature tunneling (ZCT) correction. Unlike the classical particle, a quantum particle proceeds along the path

that minimizes the action along the whole path. From a more advanced treatment, it becomes clear that the tunneling path would cut corners, *i.e.*, that a shorter path on a small expenditure of a higher barrier leads to higher tunneling rates.[31,32] This is taken into account in the small-curvature tunneling (SCT) correction,[33] which is a popular and successful method to approximate tunneling rates. Another advanced method is called instanton theory, which aims at optimization of the tunneling path, *i.e.*, finding the path with the largest tunneling probability at a given temperature. These more advanced methods are beyond the scope of this chapter.

X.3 The matrix isolation method: creating the conditions for direct observation of tunneling-driven chemistry

Matrix isolation is a technique where atoms or molecular species are trapped from the gas phase into an environment of a solidified inert gas at a temperature close to the absolute zero. By combining matrix isolation with different spectroscopic detection methods a powerful research tool has evolved over the time, which is currently being applied in several laboratories worldwide in a considerably large number of research areas. The method was in fact originally designed to study short-lived reaction intermediates, but receives nowadays many other uses, being particularly powerful for investigation of light-induced and tunneling-driven chemical reactions.

The method was first developed by the groups of Pimentel and Porter, at Berkeley (USA) and Cambridge (UK), respectively,[34,35] and its name coined in the historical single-page report by Pimentel, Whittle and Dows *"Matrix Isolation Method for the Experimental Study of Unstable Species"*, published in the Journal of Chemical

Physics, in 1954.[34] Interestingly, it took almost two decades until matrix isolation became popular among organic chemists, what happened after its success in allowing generation and characterization of the hitherto elusive cyclobutadiene molecule.[36-38]

Though as mentioned above matrix isolation was invented as a tool for stabilization, detection and characterization of reactive species, the method has also some advantages over other techniques for the study of stable molecules as well as for investigation of chemical reactions, in particular unimolecular reactions. Most of its main advantages result from the low work temperature (typically of a few Kelvin), low concentration of the trapped species, and rigidity and chemical inertness of the medium. Among these, in the context of the topic of the present chapter we may highlight: *(i)* the fact that interactions between the trapped molecules can be neglected in diluted matrices, thus allowing easy access to the study of unimolecular chemistry, *(ii)* the absence of significant perturbations of the structure of the molecules under study by the matrix environment, *(iii)* the quenching of molecular diffusion and rotation (except in the case of very small molecules), which makes vibrational spectra of matrix-isolated species being essentially pure vibrational spectra, thus enabling a direct and easy comparison with theoretically predicted spectroscopic data, *(iv)* the fact that the trapped molecules are cage-confined, which precludes occurrence of secondary cross-reactions involving species originating from different reactant molecules, and then strongly reducing the number of possible products in comparison with gas phase or solution studies, and last but not the least *(iv)* the inhibition of thermally-induced over-the-barrier processes (for barriers of just a few kJ mol^{-1}) due to the low work temperature, which opens the gate for the study of tunneling-driven reactions under favourable experimental conditions.

In spite of its power as experimental technique to address problems of structure and reactivity, matrix isolation does not require expensive equipment (Figure X.4). It shall also be noticed that, while matrix isolation has also some weaknesses, most of these have been overcome over the time by development of more reliable and precise cryostats, sample in-let systems, pressure and temperature controllers, and interfaces to spectrometers and auxiliary instrumentation, like light sources for *in situ* photolysis, pyrolysers, etc. Those less aware of the method may find detailed descriptions of the experimental setups for matrix isolation in the classic books by Meyer,[39] Andrews and Moskovits,[40] Barnes *et al.*,[41] Dunkin,[42] and Fausto,[43,44] which may be used as introductory textbooks to the technique.

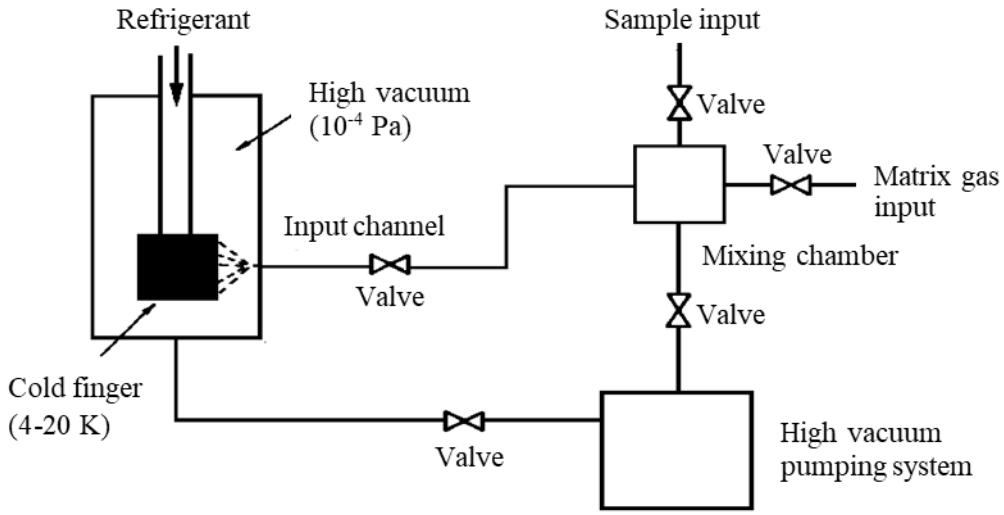

Figure X.4. Schematic representation of a basic setup for matrix isolation. The cryostat (shown on the left) shall have several external windows in order to enable to register the spectra and perform *in situ* irradiation of the sample.

An interesting feature resulting from isolation of a given chemical species in a low temperature matrix is the well-known fact that, even under well-controlled matrix deposition conditions, most of times the produced matrices allow for different local

environments around the isolated molecules. The co-existence of these different *matrix sites* leads to slightly different spectral vibrational signatures of molecules, which result in the usual observation of bands with multiplet structure (this is, however, most of times readily recognized by comparing spectra obtained using different matrix gases). As described in detail in the next sections, the local environment may change considerably the reactivity of the molecules, in particular that resulting from tunneling, and this must then be taking into account when interpreting the experimental data.

X.4 Interpretation of kinetic decays observed in cryogenic matrices

Let us consider again the case of tunneling decay of the **AH2** amino-hydroxy conformer of cytosine. For convenience, the experimentally observed amount of this form, as a function of time is depicted in Figure X.5. This decay is rather slow: during 52 hours of observation, some 66% of the initially present **AH2** conformer spontaneously converted into **AH1**. On this time scale, during registration of a single data point (taking some 3 minutes), the conformational distribution practically does not change. This permits fitting of the experimental data using different kinetic models. The tunneling conversion of **AH2** into **AH1** does not follow a first-order exponential kinetics that could be described with just one classical time constant τ_{clas}, as defined by the equation:

$$[\mathrm{n}]_t / [\mathrm{n}]_{t=0} = \exp(-t/\tau_{clas}) \qquad \text{(X.5)}$$

The fit of Eq. (X.5) to the experimentally observed decrease of **AH2** population is presented in Figure X.5a. Initially, the process is faster than predicted by the best fit

to classical single-exponential kinetics Eq. (X.5). At later stages, the tunneling clearly slows down (with respect to the best fit).[45] This suggests that the probability of tunneling depends on time.

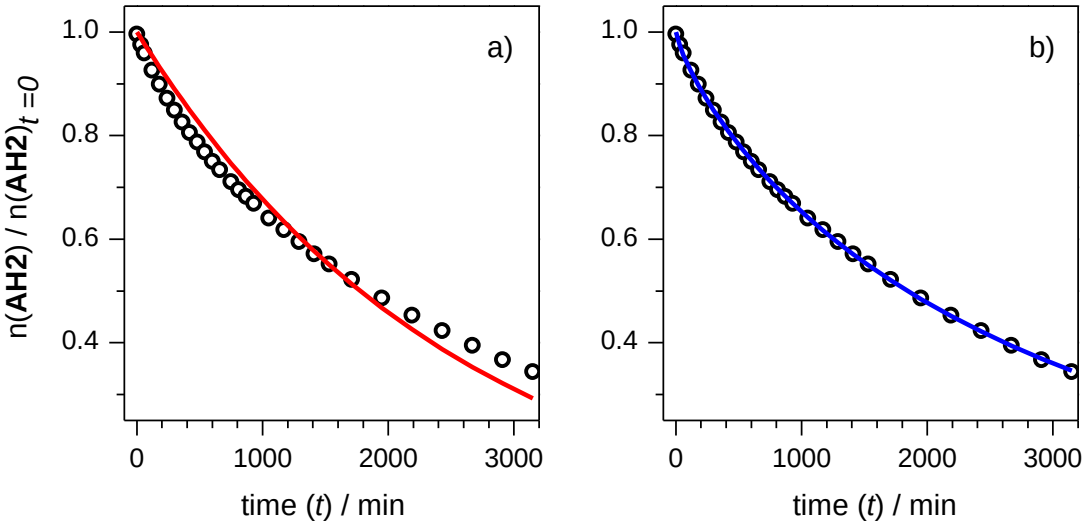

Figure X.5. Circles: evolution of the abundance of the **AH2** form of cytosine with time of keeping the matrix in the dark at 13 K. The amount of **AH2** form at the beginning of registration (t=0) is normalized to unity. Solid lines represent the best fits: (a) using the equation of classical kinetics [Eq. (X.5)]; (b) using the equations of dispersive kinetics [Eq. (X.6)] and [Eq. (X.7)]. The optimized classical time constant is τ_{clas} = 2564 min; whereas for dispersive kinetics τ_{disp}, derived from the optimized values of k and β = 0.7955 using formula [Eq. (X.7)], is τ_{disp}, = 2192 min.

Dynamical processes in which many timescales coexist are called dispersive.[46-49] The rate coefficients for dispersive processes depend on time. In the case of a chemical reaction, the time dependence of the rate coefficient, $k(t)$, termed the specific reaction rate, is rationalized in the following way. Reactions by their very nature have to disturb reactivity distributions of the reactants in condensed media, as the more reactive species are the first ones to disappear from the system. The extent

of this disturbance depends on the ratio of the rates of reactions to the rate of internal rearrangements (mixing) in the system restoring the initial distribution in reactivity of reactants. If the rates of chemical reactions exceed the rates of internal rearrangements, then the initial distributions in reactant reactivity are not preserved during the course of reactions and the specific reaction rates depend on time. Otherwise the extent of disturbance is negligible and classical kinetics, with a constant specific reaction rate, *k*, termed the reaction rate constant, may be valid as an approximation. In condensed media dispersive dynamical processes are endemic.

A cryogenic matrix represents exactly such a reaction system where the studied molecules (such as **AH2** conformer of cytosine) are embedded in a variety of different microenvironments (matrix sites), where the probability of rearrangement (*i.e.*, the reaction barrier) slightly differs from one site to another. Moreover, one may assume that the internal structure of different matrix sites in a cryogenic matrix does not change over time, which means that the chemical reaction (such as decay of **AH2** into **AH1**) proceeds on a time scale shorter than rearrangement of the matrix. Under such circumstances, the chemical reactions follow the dispersive kinetics,[50] rather than the classical first-order kinetics expected for unimolecular reactions in the gas phase. The dispersive kinetics is described by an empirical equation

$$[\mathrm{n}]_t / [\mathrm{n}]_{t=0} = \exp[-k\, t^{\beta}], \quad 0 < \beta \leq 1 \qquad \text{(X.6)},$$

introduced by Siebrand and Wildman.[51] Later Plonka showed[52] that

$$k \equiv \beta / (\tau_{\mathrm{disp}})^{\beta} \qquad \text{(X.7)}.$$

Parameter β can be treated as a measure of inhomogeneity of the matrix. Without environmental effects, β=1 should be observed, and the equation of dispersive kinetics [Eq. (X.6)] transforms into the equation of classical kinetics [Eq. (X.5)]. In matrices, β is reported to lie between 0.5 and 1, depending on the matrix, the temperature, and the time when the measurement of the kinetics is started.[53]

The progress of the **AH2** → **AH1** tunneling during the experiment is very well reproduced by Eq. (X.6), see Figure X.5b. On that basis, one can conclude that the matrix medium (even within a single, spectroscopically distinguishable site) is to some extent inhomogeneous. The value of β ≈ 0.8, obtained for the **AH2** → **AH1** tunneling at 13 K, is in accord with literature.[53,54] It suggests that, although the Ar matrix environment is not very disordered, the inhomogeneous character of this medium cannot be neglected.

It is also instructive to comment on the best fits obtained for the kinetical decays where the spectrometer-induced effect on the reaction rate is not negligible. Examples of such decays are those designated by numbers 1 and 2 in Figure X.6 (observed for pyruvic acid without filter, or with a filter transmitting up to 4200 cm^{-1}).[55] Very interestingly, such decays (that phenomenologically can be designated as “fast”) can be fitted much better with Eq. (X.5) of the classical single-exponential kinetics, as compared to purely spontaneous decays showing dispersive kinetics (which can be designated phenomenologically as “slow”). This means that the observed “fast” reactions induced by the light source of the spectrometer do not depend on the microenvironments (matrix sites). This is another practical hint for an experimentalist: true spontaneous (dark, “slow”) tunneling decays observed for matrix-isolated molecules are expected to show some dispersive character. Still, for

practical reasons, it is sometimes useful to fit the dispersive decays using the equations of classical kinetics, and in such a way obtain approximate half-life times for the studied processes.

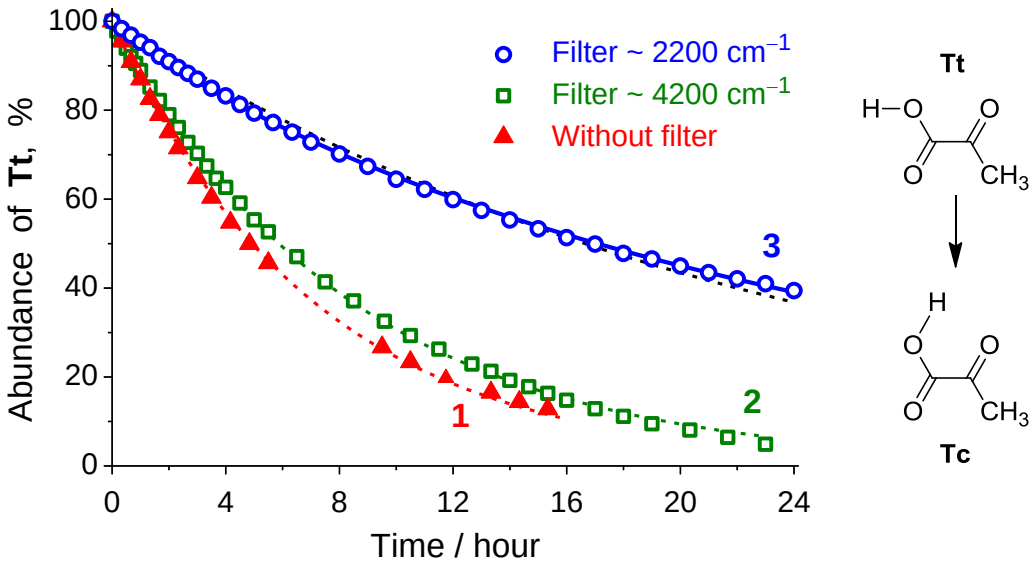

Figure X.6. Decay kinetics of **Tt** form of pyruvic acid (which converts into **Tc**) in an Ar matrix at 15 K. The spectra recorded: without filter (**1**, triangles); with cutoff filters transmitting only up to 4200 cm^{-1} (**2**, squares), or only up to 2200 cm^{-1} (**3**, circles). The dashed lines (red, green, black) show best fits using the equations of classic single exponential kinetics. The continuous line (blue) shows the best fit using the equations of dispersive kinetics.

X.5 NIR and IR-induced chemistry

To illustrate NIR and IR-induced chemistry, and also how it can interfere with the experimental observation of the tunnelling phenomenon, we start with presenting the very didactic case of the study on matrix-isolated cytosine. The results of the contemporary quantum chemical calculations[56] predict a consistent (and probably correct) energy ordering of cytosine isomers. According to these calculations, carried

out at the CCSD(T) or QCISD(T) levels, the most stable tautomer of monomeric cytosine should be the amino-hydroxy (**AH**) form. Of the two **AH** conformers, **AH1** is computed to be more stable by 3.1 kJ mol^{-1} than **AH2** (Figure X.7). The computed relative energy of the amino-oxo (**AO**) form is 5–6 kJ mol^{-1}, while those of the imino-oxo forms **IO1** and **IO2** are *ca.* 7 and 12 kJ mol^{-1}, all with respect to **AH1** (see Ref. 56 and citations therein). Hence, for the gaseous cytosine, the **AH1** and **AH2** isomers should be dominating.

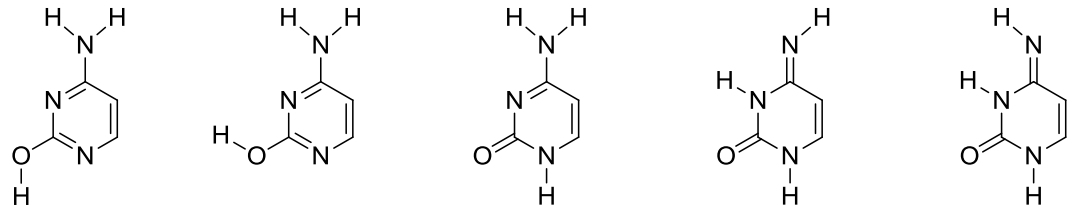

Figure X.7. Structures of the lowest-energy isomeric forms of cytosine and their relative energies (in kJ mol^{-1}) computed at the CCSD(T) or QCISD(T) levels (see Ref. 56 and citations therein).

For two conformational structures such as **AH1** and **AH2** differing only by the position of a light particle (hydrogen atom; see Figure X.7), a transformation of the higher-energy form into the lower-energy conformer can occur by tunneling. Such spontaneous transformations were observed first for formic and acetic acids isolated in low temperature matrices kept in the dark, as described later in this chapter in more detail. For cytosine, thermal equilibrium of **AH1** and **AH2** forms (differing in energy by 3.1 kJ mol^{-1}) corresponds to the population ratio **AH1**/**AH2** = 3 × 10^{13} at

13 K, and then tunneling in the dark should lead to total conversion of **AH2** into **AH1**. However, upon trapping cytosine monomers in a cryogenic matrix, the amounts of conformers **AH1** and **AH2** were monitored by IR spectroscopy and found to be approximately equal.[45]

It has been demonstrated[57] that upon narrowband near-infrared (NIR) irradiation at 7013 cm^{-1} the most stable **AH1** form almost totally converts into **AH2** (Figure X.8a; see band 1428 cm^{-1}), whereas narrowband NIR irradiation at 7034 cm^{-1} induces large-scale changes of population in the opposite direction, converting almost all **AH2** into **AH1** (Figure X.8d; see band 1439 cm^{-1}).[57]

Starting from matrices enriched either in **AH1** or **AH2** conformers, the populations of the conformers were monitored by periodical registration of spectra in the full mid-infrared range. After 2 hours, the spectrum of the sample initially enriched with **AH2** (Figure X.8a) transformed into that shown in Figure X.8b, while for the sample initially enriched with **AH1** (Figure X.8d), the spectrum after *ca.* 2 hours of monitoring is presented in Figure X.8e. The striking point is that, independently of the initial **AH1**:**AH2** ratio [very low (Figure X.8a) or very high (Figure X.8d)], the changes induced by the broadband NIR/IR light of the spectrometer source led to the same stationary state.[45] In this state, the total population of the amino-hydroxy tautomer is divided into **AH1** (53%) and **AH2** (47%) forms (see Figure X.8c and Figure X.8f). That makes the stationary **AH1**/**AH2** ratio equal to 1.1.

It is easy to prove that the conformational transformations depicted in Figure X.8, occurring on the time scale of 2 hours at 13 K are not thermally induced. This proof is based on the potential energy profile connecting the **AH1** and **AH2** conformers of cytosine (see Figure X.3).

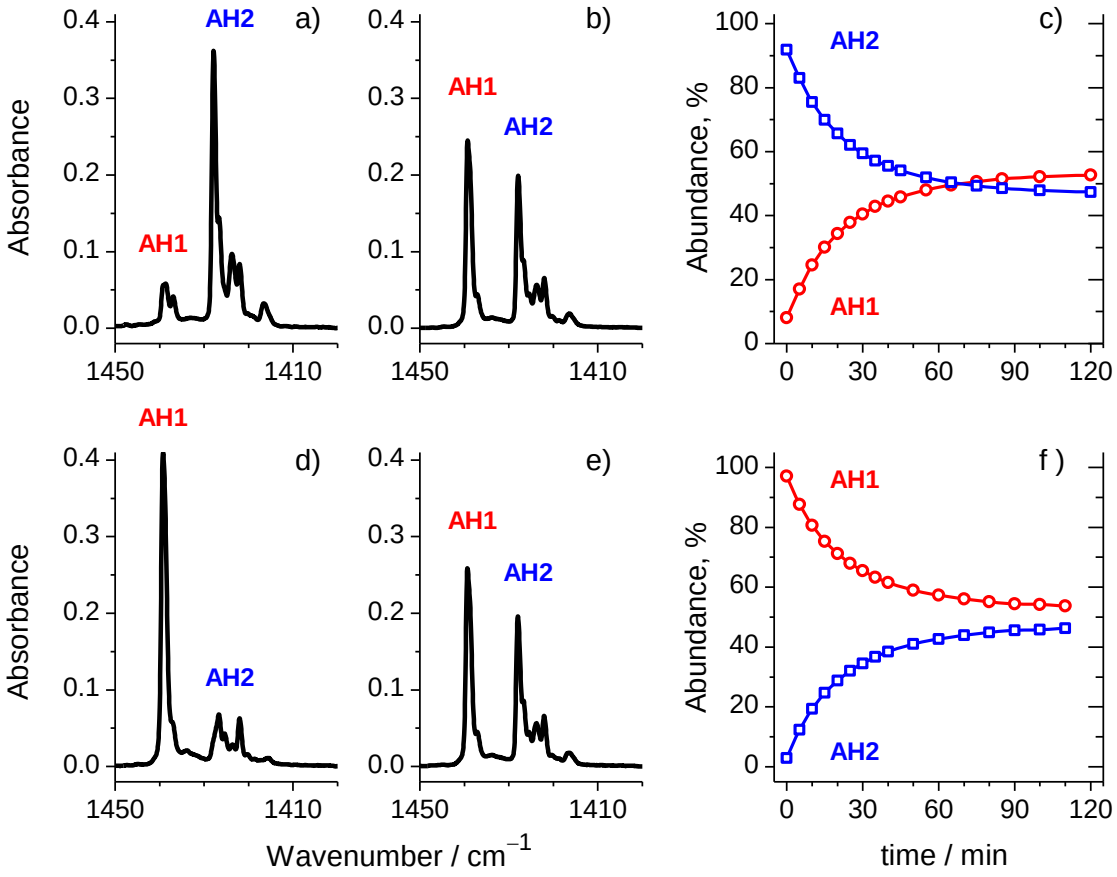

Figure X.8. Fragment of the IR spectrum of cytosine isolated in an Ar matrix at 13 K: (a) recorded after narrowband irradiation at 7013 cm^{-1}; (b) after subsequent 120 min of exposure to the NIR/IR broadband radiation of the spectrometer source; (c) evolution of abundances of **AH1** and **AH2** conformers with time of broadband NIR/IR irradiation [initial point corresponds to (a) and final point corresponds to (b)]; (d) recorded after narrowband irradiation at 7034 cm^{-1}; (e) after subsequent 110 min of exposure to the NIR/IR broadband radiation of the spectrometer source; (f) evolution of abundances of **AH1** and **AH2** conformers with time of broadband NIR/IR irradiation [initial point corresponds to (d) and final point corresponds to (e)].

If the reaction occurred in a classical way, exclusively as the thermal over-the-barrier reaction, its rate constant could be estimated using the Eyring-Polányi equation,

$$k = \frac{\kappa k_B T}{h} e^{-\frac{\Delta^{\ddagger} G^{\ominus}}{RT}} \qquad \text{(X.8)},$$

where k is the reaction rate (in s^{-1}), κ is the transmission coefficient usually assumed to be 1 (no tunneling and no reflection at the barrier top), k_B is the Boltzmann constant (1.38×10^{-23} J K^{-1}), T is the absolute temperature (in K), h is the Planck constant (6.626×10^{-34} J s^{-1}), R is the universal gas constant, and $\Delta^{\ddagger}G^{\ominus}$ is the standard Gibbs energy of activation of the studied compound.

For cytosine, the theoretical harmonic vibrational computations at the B3LYP/6-31++G(d,p) level give $\Delta^{\ddagger}G^{\ominus}$ = 34.6 kJ mol^{-1}. The half-life of the **AH2** → **AH1** over-the-barrier reaction is calculated to be ca. 10^{120} years at 13 K (in contrast, the estimated half-life for the same reaction would be about 130 ns at 298 K).

In order to investigate in more detail the **AH1** ↔ **AH2** phototransformation induced by broadband NIR/IR light, several bandpass IR filters were employed.[45] Whatever the initial **AH1**:**AH2** ratio, no measurable change in relative populations of these forms was observed (during 10–30 min) for matrix-isolated cytosine exposed to the light of the spectrometer source passed through a filter transmitting only below 1750 cm^{-1} (equivalent of 21 kJ mol^{-1}). However, when this IR filter was substituted by another one transmitting light in the spectral range up to 4200 cm^{-1} (50 kJ mol^{-1}), quite rapid changes in the **AH1**:**AH2** population ratio were observed.[45] These observations demonstrate that not only NIR excitation to overtones (at 7013 or 7034 cm^{-1}) but also excitation of the fundamental OH or NH stretching modes (in the 3610−3430 cm^{-1} range) induces mutual conversion of **AH1** and **AH2** conformers. This can be rationalized by considering that the conformational change induced, *e.g.*,

by the excitation at 3601 cm^{-1} (to the first excited state of the OH stretching vibration in **AH2**) should be an over-the-barrier process. The energy of this excited vibrational state (3601 cm^{-1} is ca. 43 kJ mol^{-1}) is indeed higher than the barrier for the **AH2** → **AH1** conversion, estimated at the B3LYP/6-31++G(d,p) level to be 34.6 kJ mol^{-1}.[45]

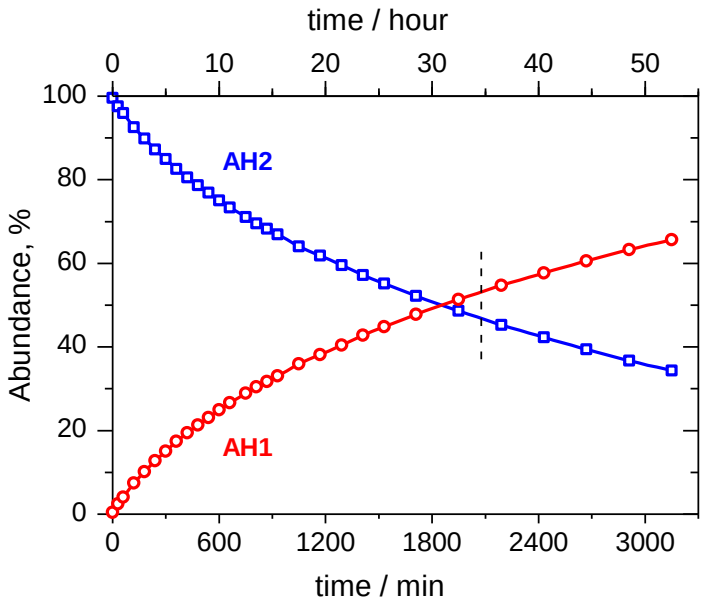

Figure X.9. Evolution of abundances of **AH1** and **AH2** forms of cytosine with time of keeping the matrix in the dark at 13 K and monitoring only through a filter transmitting below 1750 cm^{-1}; the initial population of **AH1** (near 0%) and **AH2** (near 100%) was induced by narrowband NIR irradiation at 7013 cm^{-1}. The vertical dashed line near 35 h corresponds to the conformer distribution shown in Figure X.8b and Figure X.8e. The continuous lines, connecting the experimental points, are shown to guide the eye.

For matrix-isolated cytosine kept in the dark and monitored only in the spectral range below 1750 cm^{-1} (with photons of the spectrometer source having energies no more than 21 kJ mol^{-1}), relative populations of **AH1** and **AH2** changed very slowly. Independent of the initial **AH1**:**AH2** ratio, the higher-energy **AH2** conformer always converted into **AH1**. In order to observe the changes of relative populations of **AH1**

and **AH2** in a possibly largest scale, in a dedicated experiment, a matrix with very high relative population of **AH2** (with the **AH1** amount close to zero) was prepared by narrowband irradiation at 7013 cm^{-1}. After 35 hours of monitoring, the **AH1**:**AH2** ratio reached the value of 1.1, and continued to grow (Figure X.9). After 52 hours in the dark, the **AH1**:**AH2** ratio was approximately 2, and the kinetical profiles did not show any sign of reaching a plateau.[45] Such a kinetical behaviour is pointing out to the occurrence of a tunneling process.

The spectrometer-induced conformational changes and tunneling effects, similar to those observed for the parent cytosine, were also observed for several 5-substituted cytosines,[58] and these cases by no means constitute an exception. The spectrometer-induced structural changes in matrix-isolated molecules do indeed occur frequently and should be carefully characterized, in order to be able to separate them from the spontaneous changes (that typically occur on a larger time scale). Here we shall provide some more examples.

We have recently studied in detail the conformational behaviour of matrix-isolated pyruvic acid.[55] It has two main conformational structures, designated as **Tc** and **Tt** (Figure X.10).

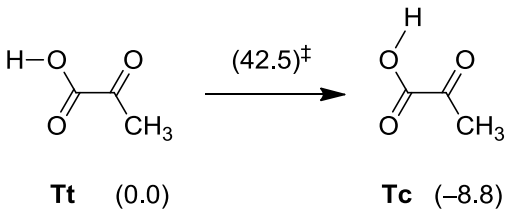

Tt (0.0) **Tc** (–8.8)

Figure X.10. Two main conformers of pyruvic acid and their ZPE-corrected relative energies (kJ mol^{-1}) computed at the B3LYP/6-311++G(d,p) level, with respect to the minor **Tt** form. The ZPE-corrected relative energy of the transition state (with respect to **Tt**) for intramolecular torsion of the OH group is shown above the arrow.

The main **Tc** form of pyruvic acid is almost exclusively present in the gas phase and in freshly deposited cryogenic matrices. Irradiation of the samples at the frequency of the first OH stretching overtone of **Tc** (at 6630 cm^{-1}) results in conformational isomerization, and up to 75% of the compound is transformed into its higher-energy **Tt** conformer. This allowed for the subsequent studies of kinetics of spontaneous and spectrometer-induced conformational changes. Once the **Tt** form was generated, several independent experiments were performed. In one case, the sample was exposed to the unfiltered IR beam of the spectrometer. In other cases, a long-pass cutoff IR filter was placed between the spectrometer source and the sample. Two different cutoff filters were applied: transmitting only light with wavenumbers up to 4200 cm^{-1} (~50 kJ mol^{-1}) or up to 2200 cm^{-1} (~26 kJ mol^{-1}). In all cases the **Tt** → **Tc** decay process was followed spectroscopically over the time. The decay rates in these experiments depended on the applied filter range (Figure X.6, Section X.4).[55]

In the experiments undertaken without filter or with filter transmitting in the whole mid-IR range (transparent up to 4200 cm^{-1}), a half of **Tt** form was converted to **Tc** during 5 or 6 hours. In the case of the filter transmitting only light up to 2200 cm^{-1} the decay was considerably slower: it took ~17 h to convert a half of **Tt** form back to **Tc**. The rationalization of the observed differences is the following: when the matrix sample is protected with the long-pass cutoff filter, transmitting only below 2200 cm^{-1}, all accessible energy levels in the system are below the barrier (for each conformer) and isomerization from **Tt** to **Tc** is only feasible *via* tunneling.[55] With the filter transparent up to 4200 cm^{-1}, or without it, excitation of the OH stretching fundamental modes, promotes additional phototransformations. In this case, the

stationary state is strongly shifted toward **Tc**. Comparing the present case of pyruvic acid with the case of cytosine discussed earlier, there is similarity: only with a proper filter (having its cut-off below the activation energy) the true tunneling kinetics can be observed.

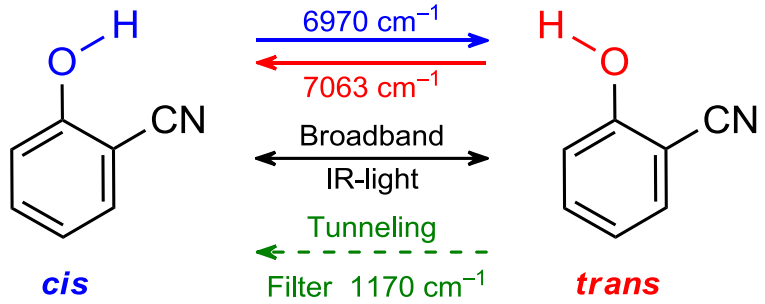

Figure X.11. Narrowband-induced (top), broadband-induced (middle) and tunneling isomerizations in matrix-isolated 2-cyanophenol. The observation of tunneling was only possible by using a longpass cutoff filter transmitting solely below 1170 cm^{-1}.

Some other interesting cases related to spectroscopic studies of H-atom tunneling concern cyanophenol[59] and imino-thiol forms of acetamide.[60] In cyanophenol (Figure X.11), the barrier separating the higher energy *trans* form from the conformational ground state *cis* is computed to be lower than 15 kJ mol^{-1} (1250 cm^{-1}). In agreement with such a low energy barrier, a successful spectroscopic observation of the *trans* → *cis* tunneling relaxation was only possible by using the longpass cutoff filter transmitting solely below 1170 cm^{-1}.[59]

Based on all the cases described above, we propose here an empirically derived "rule of thumb" for spectroscopic observation of tunneling decays. This rule, up to date, has been in agreement with all our experimental observations. According to this rule, the calculated activation energy will approximately define the higher bound

of the cutoff value of the longpass filter that should permit spectroscopic characterization of the expected tunneling reaction, without affecting the kinetics of the spontaneous reaction. It is important to keep in mind that when the relative energies of transition states (with respect to the neighbouring minima) fall into the mid-IR range of the spectrum, the possibility of IR-induced photochemistry (during recording of spectra) should not be neglected.

X.6 Conformational isomerizations by tunneling

Numerous investigations on tunneling-driven reactions of organic molecules observed in low temperature matrices refer to conformational isomerizations. The prototype reaction was observed for the first time for formic acid (HCOOH; see Figure X.12).[61-63] The most stable *Z* (*cis*) conformer of this compound was isolated in an argon matrix and vibrationally excited by narrowband NIR light tuned at the frequency of the first overtone of its OH stretching vibration (6934 cm^{-1}), which led to generation of the less stable *E* (*trans*) conformer. The *cis* conformer was then found to convert back to the *trans* form by tunneling at a rate of *ca*. 4 x 10^{-3} s^{-1}.[61]

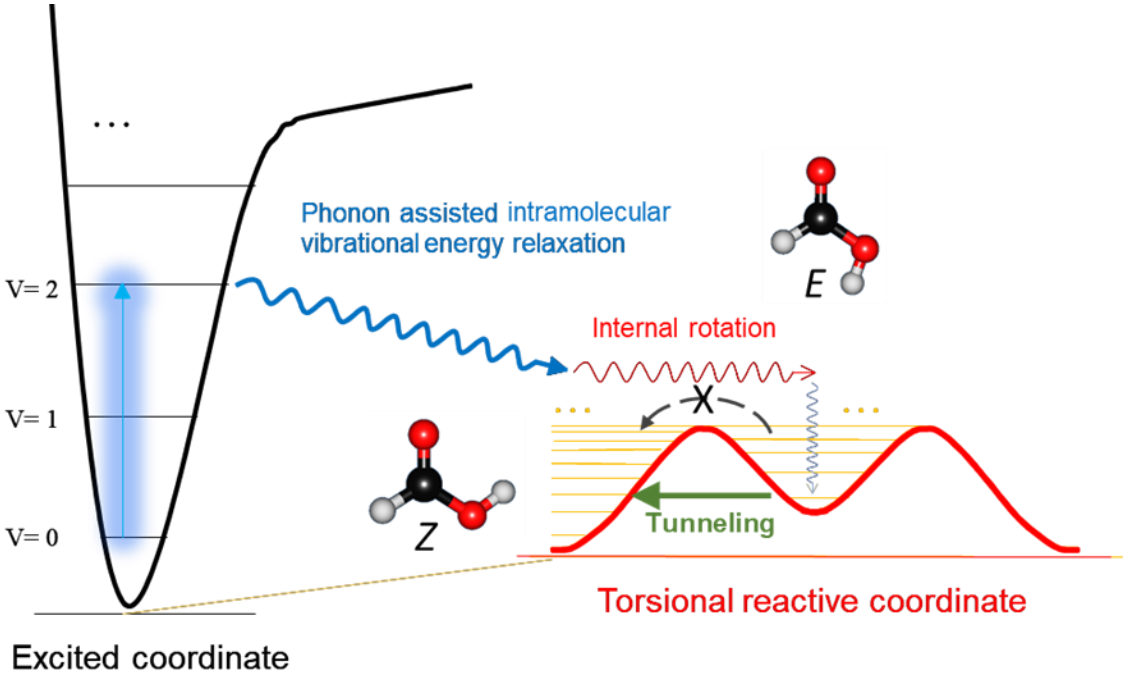

564
565
566 **Figure X.12.** Conformers of formic acid and schematic representation of the
567 (N)IR-induced *Z (cis)* → *E (trans)* isomerization and subsequent decay of the *E*
568 conformer into the more stable *Z* form by tunneling (green arrow). The
569 photoisomerization involves vibrational excitation of a high-absorption-cross-section
570 high-energy mode, followed by phonon assisted intramolecular vibrational energy
571 relaxation and internal rotation. The over-the-barrier thermal back-isomerization is
572 not accessible. Note that the *cis*/*trans* designation of the conformers does not follow
573 some of the original publications, where the opposite designations are used.

574

575 Interestingly, the photogeneration of the *trans* conformer from the *cis* form was
576 observed to take place even when irradiation of the lower energy form was
577 performed with an energy below the energy barrier separating the two conformers
578 (Figure X.13).[64] This observation implies that, in those cases, vibrational excitation of
579 the *cis* conformer followed by vibrational energy relaxation takes the molecule to a
580 high vibrational excited torsional state, reducing the height and width of the energy
581 barrier for conformational isomerization in such a way that the transformation can
582 then take place by tunneling.

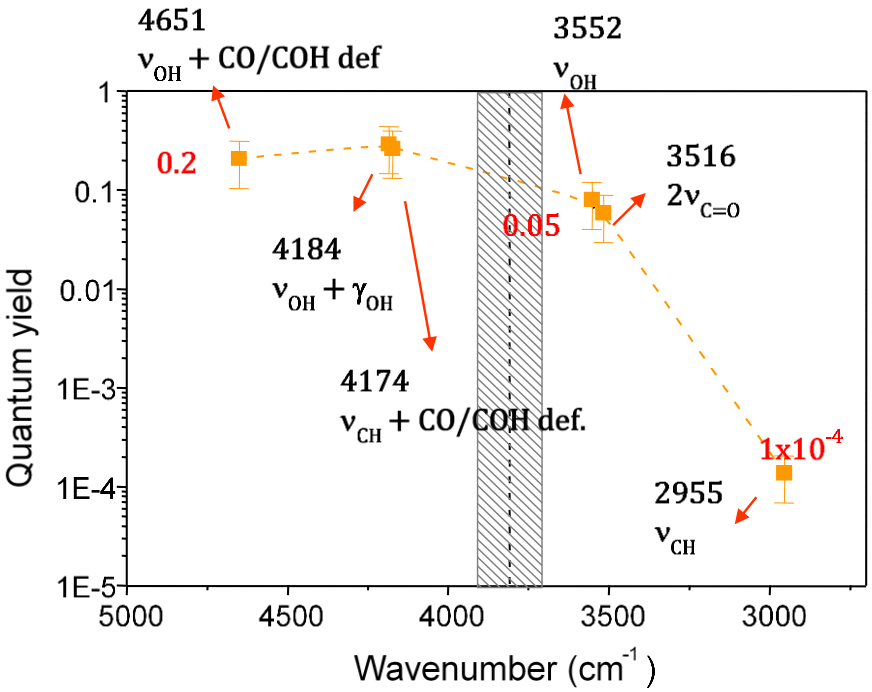

583

584

585 **Figure X.13.** Quantum yields for the conversion of the *Z* conformer of formic acid
586 into the *E* form upon vibrational excitation at different frequencies. The quantum
587 yields are indicated in red, while the excitation wavenumbers and description of
588 excited modes are shown in black. The grey area corresponds to the range of
589 energies (in cm^{-1}) of the available data on barrier for $Z \rightarrow E$ internal rotation. Adapted
590 from Ref. 64 with permission of the American Chemical Society. Copyright 2003.

591

592 The selective photogeneration of high-energy conformers that are found in nature in
593 very low amounts (or not found at all) by vibrational excitation of the low-energy and
594 abundant in nature forms has more than academic significance: it also opened the
595 opportunity to investigate the characteristic chemistries of species otherwise not
596 accessible to experimentation, which might be different from those of the low-energy
597 conformers. In the case of formic acid, for example, it was found that, while the more
598 stable *cis* conformer photochemically decomposes predominantly to carbon
599 monoxide and water, the less stable *trans* form dissociates mainly to carbon dioxide

and molecular hydrogen.[65] This experimental approach has been evolved over time and, recently, we have introduced the concept of *vibrational antenna* to control the structure of a fragment remotely located in the molecule relative to the group where the energy is introduced (the *antenna*),[66-68] and also presented the first example where excitation of the second OH overtone was used to promote conformational changes,[69] thus demonstrating the feasibility of this type of excitation to promote structural changes in a molecule. Use of higher-order overtones allows for the introduction in a molecule of a large amount of energy (~10500-6300 cm^{-1}, or ~130-120 kJ mol^{-1} upon excitation of the second OH stretching overtone, *vs.* ~7300-6300 cm^{-1}, or ~87-75 kJ mol^{-1} upon excitation of the first OH stretching overtone), thus opening the gate to the promotion of chemical processes having considerably higher barriers than those accessible hitherto.

Many other molecules containing a carboxylic acid group have been studied following a similar approach to that initially used to investigate the higher energy conformer of formic acid. These include acetic and propionic acids,[70-73] halogenated acetic acids,[74-77] α-hydroxyl, α-keto and α,β-unsaturated carboxylic acids,[55,67,78-83] aromatic and other cyclic carboxylic acids,[84-89] dicarboxylic acids[90-94] and amino acids.[95-101] In most of those cases, the higher-energy conformers generated *in situ* by IR excitation of lower-energy forms were found to relax in the dark, by tunneling, to the latter forms.

An interesting example of the combined use of selective IR irradiations triggering conformational isomerization and tunneling decay of the photogenerated higher-energy conformers has been reported as a way to selectively produce the four conformers of propionic acid.[73] Propionic acid has two low-energy conformers, **Cs** and **Cg**$^{\pm}$, where the carboxylic group assumes the *cis* configuration, and two high-

energy forms, **Ts** and **Tg$^{\pm}$**, where the conformation of the carboxylic group is *trans* (Figure X.14). In the vapour of the compound at room temperature, the two low-energy conformers exist in equilibrium. During deposition of the compound in an argon matrix, the **Cg$^{\pm}$** conformer converts into the lowest energy **Cs** form, in an over-the-barrier process made accessible due to local heating of the cold substrate resulting from the landing of the molecules of the gaseous beam being deposited (conformational cooling).[102,103] This leads to the sole presence of the **Cs** conformer in the initially deposited matrix. Selective NIR irradiation at the frequency of the first OH stretching overtone of this conformer results in production of both **Ts** (through rotation around the C–O bond) and **Cg$^{\pm}$** (*via* rotation around the α C–C bond) (Figure X.14). If subsequently the sample is left in the dark, the **Ts** form relaxes by tunneling back to the initial conformer (**Cs**) in a few minutes, since this conversion requires only movement of the light hydrogen atom, while the **Cg$^{\pm}$** form persists in the matrix for several hours (tunneling to the only conformer with a lower energy than the **Cg$^{\pm}$** form, *i.e.*, the most stable **Cs** conformer, has a very low probability since it implies movement of a heavy fragment; the slow decay observed for this conformer results from its isomerization to **Cs** over the very low energy barrier (0.7 kJ mol^{-1}) separating these two forms). The population of the **Cg$^{\pm}$** conformer can then be increased by repeating the procedure making this form the dominant one in the matrix. Subsequently, the **Cg$^{\pm}$** conformer can be selectively excited, by pumping its OH stretching overtone. Such excitation results partially in regeneration of the **Cs** conformer (*via* rotation about the C–C bond α to the carbonyl) and partially in the production of the highest energy **Tg$^{\pm}$** conformer (by rotation around the C–O bond). As a whole, these experiments allow to generate selectively and undertake the experimental characterization of all the four conformational states of propionic acid.

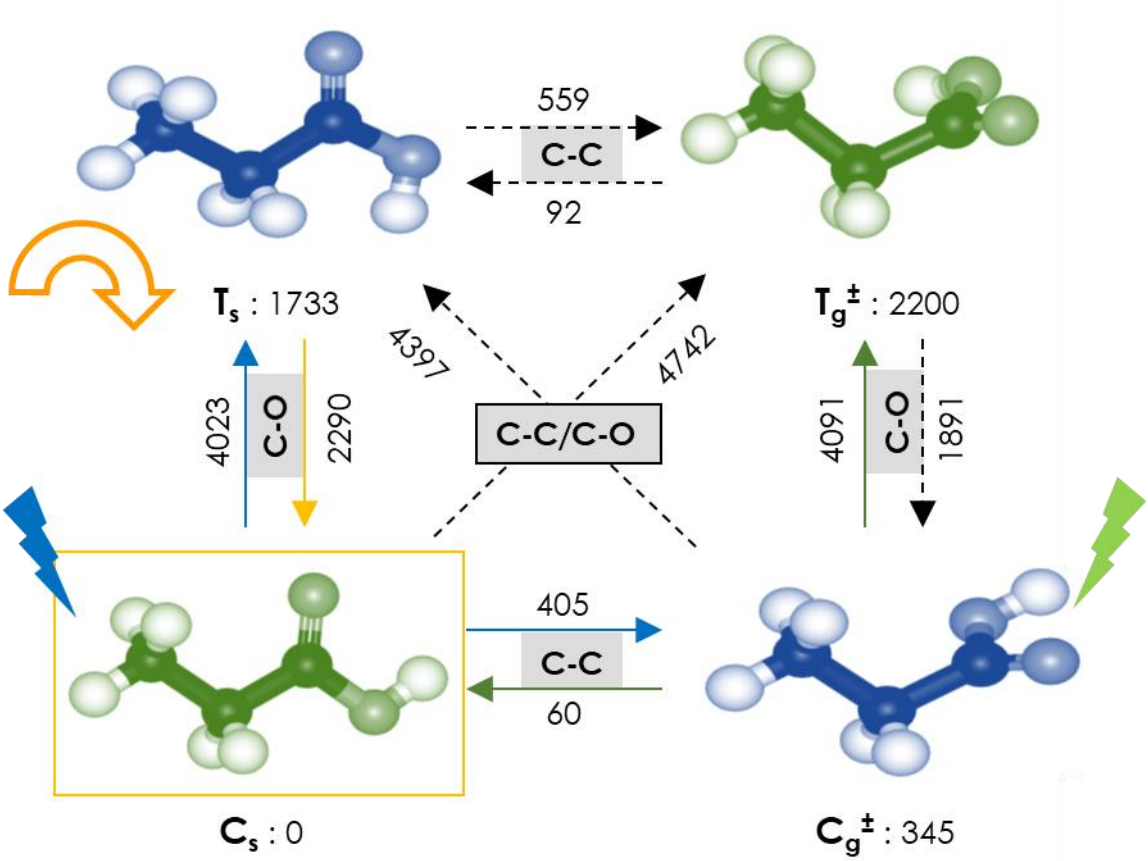

Figure X.14. Conformers of propionic acid, their relative stabilities and barriers for conformational isomerization (both in units of cm^{-1}) about the C–O and C–C(O) bonds. The figure also illustrates the effect of combination of selective NIR excitation and tunneling decay processes leading to observation of the four conformers of propionic acid isolated in solid argon. The flash-type arrows indicate NIR irradiations performed at the first OH stretching overtone of the conformer, resulting in the transformations indicated by the solid arrows of the same color. The arch-type arrow indicates tunneling. Note the different notation of the conformers used here when compared with that used in the original reference. Adapted from Ref. 73 with permission from the American Chemical Society. Copyright 2005.

A very interesting phenomenon that has been taken advantage of, in order to investigate high-energy conformers of carboxylic acids, is the fact that the stability of these conformers often strongly increases in matrices made by materials which are able to interact in a specific way with the carboxylic acid group, in particular

molecular nitrogen.[55,78,79,104,105] Specific interactions between the matrix N_2 molecules and the OH acid group of the carboxylic fragment have been in fact shown to increase the lifetime of the otherwise short-lived conformers of this type of molecules, by establishing an $OH\cdots N_2$ hydrogen bond type interaction whose interaction energy is typically of *ca.* –5 kJ mol^{-1}.[104,106] This interaction energy may be compared to that associated with the $OH\cdots Ar$ interaction reported by Wawrzyniak *et al.*,[107,108] who found that the latter amounts only to –1.5 to −2.0 kJ mol^{-1}.

The stabilizing effects due to the $OH\cdots N_2$ interaction are in fact frequently very large, while in general the matrix material can considerably influence the tunneling decay rates, even when we are considering only noble gas matrices. Clearly, in addition to the barrier-height change upon solvation in polarizable media or due to specific interactions with the matrix material (like in the case of N_2), other factors can also influence the tunneling rates. Among these we can mention the coupling between vibrational levels involved in the energy relaxation process, and the magnitude of the energy gap between the tunneling levels (which leads to changes in the order of the phonon process providing the required energy dissipation).[62,109,110] For formic acid, the decay rate in a nitrogen matrix is smaller by 5, 30, ~55 and 10 000 times compared to xenon, krypton, argon and neon matrices, respectively.[62,111] For acetic acid, it is slower in N_2 matrices by a factor of ~600 than in both argon and krypton matrices and by a factor of 3000 than in a xenon matrix.[72]

The stabilization of high-energy conformers in an N_2 matrix may even lead to a completely different pattern of reactivity compared to argon or other noble gases. A remarkable case was found for 2-fluorobenzoic acid (2FBA),[84] and very interesting results have also been reported for glycolic acid[82] and β-aminoisobutyric acid,[95] the reader is invited to consult original articles for details.

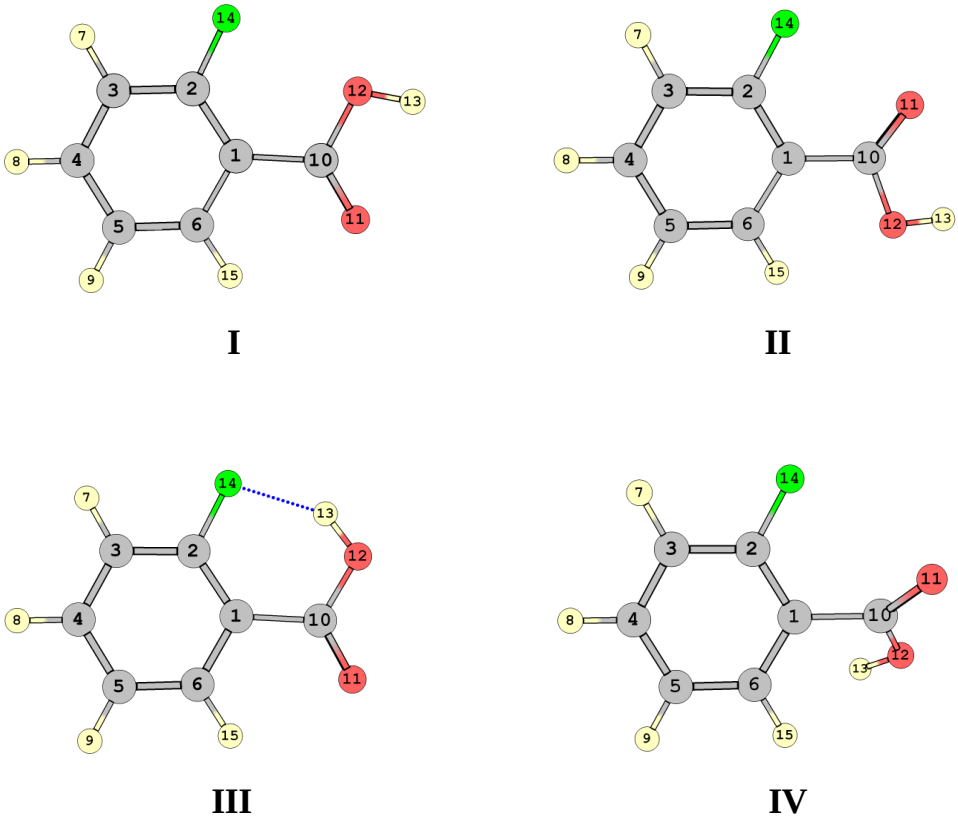

Figure X.15. Conformers of 2FBA. Conformer **IV** has a non-planar geometry and the represented structure has a symmetry-related counterpart. Reproduced from Ref. 84 with permission from the American Institute of Physics. Copyright 2017.

The molecule of 2FBA has an asymmetric substitution pattern at the ortho positions (on one side a fluorine atom, and on the other a hydrogen atom). This leads to very different intramolecular interactions when the orientation of the carboxylic group changes. The molecule may exist in four different conformers (Figure X.15), two of them bearing the carboxylic acid group in the *cis* conformation (the most stable forms) and the other two exhibiting this group in the *trans* conformation. The *cis* conformers (**I** and **II** in Figure X.15) account for *ca.* 98% of the total population in the gas phase at 25 °C, the calculated **I**:**II** population ratio being ~3.[84] The third conformer on the increasing order of energy (**III**) is stabilized by an intramolecular

OH···F hydrogen bond and has an estimated population at 25 ºC of *ca.* 2%, while conformer **IV** has a high relative energy (~30 kJ mol^{-1}) and should have a negligible population in the same conditions.[84]

As expected, no bands ascribable to the higher-energy *trans* conformers (**III**, **IV**) were observed in the spectra obtained for the compound in argon or N_2 matrices. Narrowband NIR irradiations at the frequencies of the first overtone of the O–H stretching vibration of conformers **I** and **II** were performed.[84] In the argon matrix, irradiations at the frequencies corresponding to conformer **I** resulted in selective conversion of this form into conformer **III** (rotation around the C–O bond), while those performed at the characteristic frequencies of conformer **II** appeared to be unable to promote any conformational transformation, since no spectral changes could be observed (Figure X.16). This result was *a priori* unexpected, since one could expect that conformer **II** should convert into conformer **IV** (which differs from **II** by rotation around the C–O bond), in a process similar to that corresponding to the **I**→**III** transformation. The results obtained in the N_2 matrix were also surprising: irradiations at frequencies of the vibrations of conformer **I** yielded identical results as in the argon matrix (conversion of conformer **I** into **III**), but, this time, excitation of conformer **II** resulted in the conversion of this conformer into conformer **III** (Figure X.16). A point to note is that this last process (**II**→**III**) was found to be considerably less efficient than the **I**→**III** conversion.

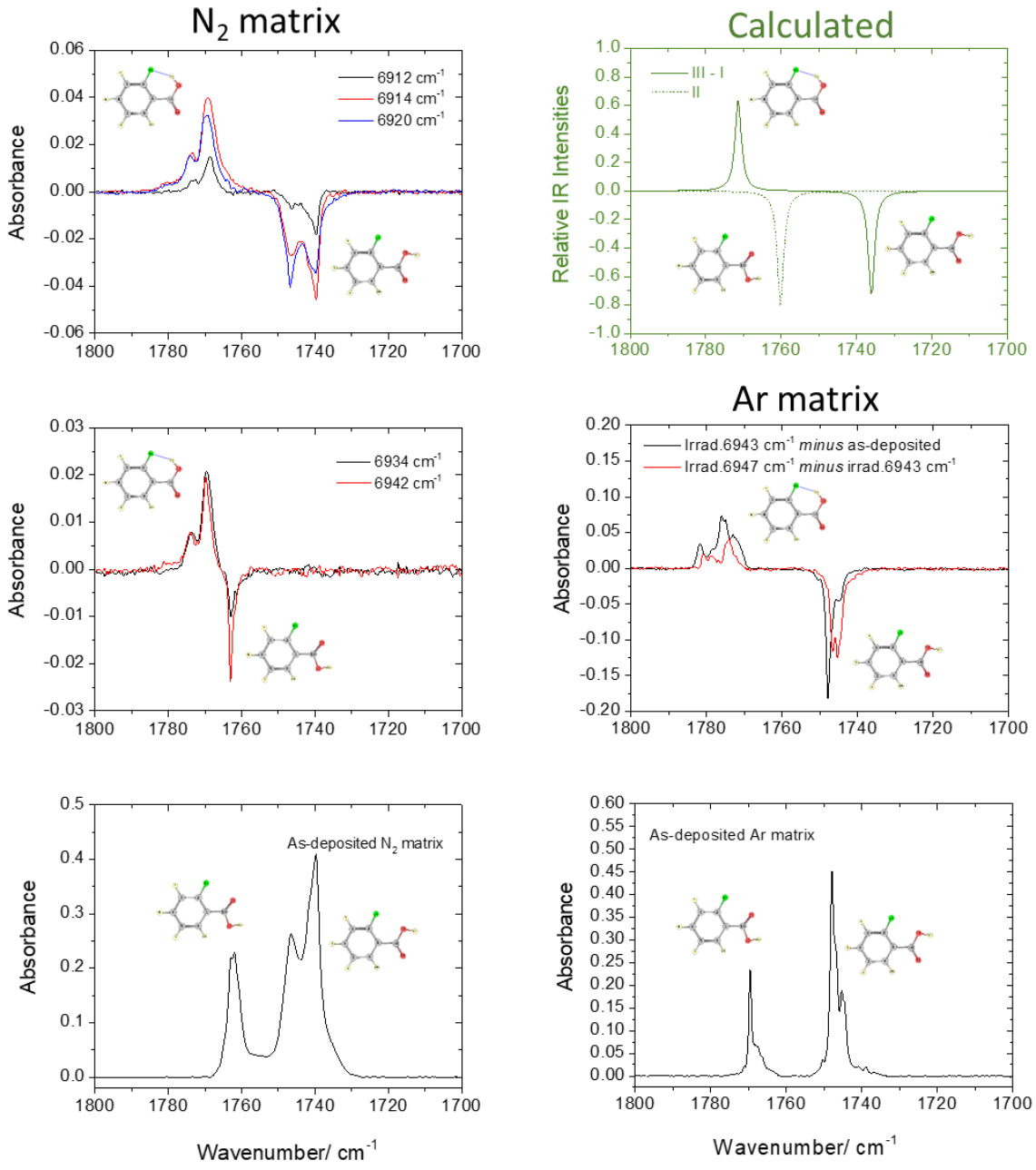

Figure X.16. (*Right top; green*) Simulated IR difference spectrum: B3LYP/6-311++G(d,p) calculated spectrum of conformer **III** *minus* calculated spectrum of conformer **I** (solid line) in the C=O stretching region; the calculated spectrum of conformer **II** in the same spectral region is shown by the dotted line. *(Right middle)* IR difference spectra of 2FBA showing the results of the performed irradiation experiments carried out in an argon matrix. (*Right bottom*) Spectrum of the as-deposited 2FBA argon matrix. *(Left top and middle)* IR difference spectra of 2FBA showing the results of the performed irradiation experiments carried out in solid N_2, by irradiating at frequencies of bands of conformer **I** and **II**, respectively (Left b*ottom*) Spectrum of the as-deposited 2FBA N_2 matrix. Reproduced from Ref. 84 with permission from the American Institute of Physics. Copyright 2017.

The key information to understand these results relates with the relative size of the barriers to internal rotation around the C–O bond in conformers **III** and **IV** (the first is 3 times higher than the second (40.4 kJ mol^{-1} vs. 13.9 kJ mol^{-1}) due to the presence in conformer **III** of the stabilizing O–H···F intramolecular H-bond interaction that is absent in conformer **IV**) and the very small energy barrier associated with the **IV**→**III** isomerization (2.6 kJ mol^{-1}),[84] besides the stabilization of high-energy conformers resulting from the O–H···N_2 interaction in the nitrogen matrix.

In the argon matrix the low energy barrier for the **IV**→**II** process allows the fast tunneling conversion of **IV** into **II** to take place once the higher energy conformer (**IV**) is produced by vibrational excitation of **II**. It shall be noticed that conformer **IV** has a non-planar geometry, with the COOH group twisted out of conjugation with the ring. This means that the H-atom tunneling within the carboxylic group has to be followed by a relaxation of the geometry leading to the planar conformer **II**. This structural relaxation involves movement of heavy atoms, so that tunneling is not favoured. Nevertheless, the required structural relaxation is barrierless, so that it takes place promptly following the hydrogen tunneling. In this way, observation of **IV** is precluded. On the other hand, the high-energy barrier associated with the **III**→**I** conversion makes this process inaccessible and allows the observation of conformer **III**. In contrast, in the N_2 matrix, the stabilization of the initially formed conformer **IV** after pumping of **II** resulting from OH···N_2 specific interactions allows this conformer to survive long enough to allow the **IV**→**III** over-the-barrier conversion to be competitive with the **IV**→**II** tunneling. Hence, while part of the initially formed conformer **IV** still converts back to **II** by tunneling (justifying the low efficiency of the observed **II**→**III** transformation), the remaining fraction of **IV** converts to **III**,

762 explaining the observed neat conversion of the NIR excited conformer **II** into form **III**
763 in the N_2 matrix.

764 Another way to promote stabilization of otherwise short-lived conformational species
765 of carboxylic acids is to quench the tunneling by making associates with other
766 molecules or forming dimers of the compound. There are two different approaches to
767 perform this type of studies. In one type of experiments, the compound to be studied
768 is deposited together with the molecule chosen to form the complex and the higher-
769 energy conformers are then produced *in situ* by selective NIR irradiation of the stable
770 precursor conformers. Thermal mobilization by annealing of the matrix at higher
771 temperatures allows for diffusion of the molecules and formation of the associates
772 containing the high-energy forms. The alternative procedure involves co-deposition
773 of the compound under investigation and the complexing molecule in such conditions
774 that they associate (for example depositing the matrix at a higher temperature or
775 preparing concentrated matrices). The associates will have the molecule under study
776 in one of its low-energy conformers, which is initially present in the gaseous mixture
777 being deposited. Then, selective NIR irradiation of the associates may be used to
778 generate complexes where the compound adopts one of its high-energy
779 conformational states. In case of dimers, the ligand molecule is, obviously, the
780 molecule under study itself, but the experimental procedures are similar. Both
781 approaches were used very successfully to generate a plethora of new dimers of
782 formic acid and acetic acid containing the higher-energy *trans* conformer of these
783 molecules,[105,112-113] as well as associates of these acids with water.[114,115] All
784 complexes where the OH carboxylic moiety is involved in the intermolecular
785 interaction that gives rise to the associate were found to be stable or at least
786 considerably more stable than the corresponding monomeric species, clearly

demonstrating that the probability of tunneling strongly reduces upon association. For example, the *trans* formic acid complex with water in an argon matrix is stable for months, in contrast with the *trans* formic acid monomer, whose lifetime is only of about 9 minutes.[114] Also, dimers of either formic or acetic acid bearing a *trans* unit in their structures participating in an intramolecular H-bond were found to be stable.[113-115] The main factor responsible for reducing the tunneling probability is the increase in the barrier height for internal rotation around the C–O bond resulting from the participation of the carboxylic group in a specific H-bond interaction with the ligand. However, also when the OH fragment does not participate directly in the intermolecular bonding, complexation was observed to decrease the tunneling probability, and dimers of formic acid and acetic acid matching this condition were found to have tunneling decay rates considerably lower than the corresponding monomers under the same experimental conditions.[113-115] In these cases, it is clear that a stabilization due to the increase of the barrier height cannot explain the observations. We can speculate that, since the tunneling barrier is influenced by the matrix environment (as pointed out in the section X.4, tunneling in general obeys a dispersive type kinetics and molecules trapped in different sites may decay at considerably different rates), the dissimilar morphologies of the matrix-sites required to accommodate the monomer and the dimers are such that they tend to favour the tunneling in the monomer case, but an accurate description of this effect is a complicated theoretical task and a convincing explanation for the experimental observations is still missing.

Conformational isomerization by tunneling can also occur for molecules other than carboxylic acids, but a large number of the reported cases involve the rotamerization of the O–H moiety. In previous sections the case referring to the amino-hydroxy

812 conformers of cytosine[58] has already been discussed in some detail, and this
813 phenomenon has also been observed for some cytosine derivatives[58] and, recently,
814 for 9-methylguanine.[116] Other types of molecules where conformational isomerization
815 by tunneling has been reported are asymmetrically substituted phenols,[59,117-121] and
816 derivatives of carbonic acid.[122] However, recently, we have reported the first case
817 where the conformational transformation involves rotamerization, by tunneling, of an
818 S–H moiety.[60] Such possibility could be expected based on the structural similarity
819 between the molecules containing the O–H fragment and their sulphur analogues,
820 but it had never been observed experimentally before our study.

821 In order to observe conformational transformations by tunneling, as explained above,
822 one has to generate the higher-energy conformers that can then decay to more
823 stable forms. In the examples given in this section for carboxylic acids, the
824 production of such higher-energy conformers was achieved by *in situ* selective
825 vibrational excitation of lower energy forms. An alternative possibility is to generate
826 these conformers as result of UV irradiation either of a lower energy conformer of the
827 same molecule or of a different precursor molecule. In the first case, the
828 rotamerization may take place either in an excited state or in the vibrationally hot
829 electronic ground state after electronic relaxation. Though these two possibilities are
830 not easy to distinguish, the observation of the same conformational transformation
831 upon both UV and IR excitation in keeping the experimental conditions similar, points
832 to the occurrence of the transformation in the ground electronic state, while the
833 opposite is valid for those transformations that occur only upon UV excitation. *i.e.*,
834 the rotamerization with all probability takes place in an excited electronic state. The
835 situation for the cases where the high-energy conformers result from a
836 rearrangement of different precursor molecules are more complex because they

frequently involve a multistep mechanism, *e.g.* bond-breaking leading to formation of radical pairs followed by recombination of the radicals at the same atoms (but with an orientation different from the original one) or involving different atoms, after spin redistribution in one or both radicals undergoing recombination. All the cases mentioned above fit one or other of these possibilities. A common pattern is, naturally, the subsequent decay of the initially generated high-energy conformers into lower-energy forms through the tunneling mechanism.

The conformational transformation we have recently reported as the first experimentally observed tunneling rotamerization of an S–H moiety[60] involved the initial photogeneration of the imino-thiol isomeric forms of thioacetamide as result of UV-induced rearrangement of the most stable amino-thione form of the compound. Four different imino-thiol forms were generated, corresponding to the *cis* or *trans* thiol (C/T) conformers of the two imino isomers (*syn* and *anti*; s/a) (Figure X.17).

The *syn-cis* (**sC**) imino-thiol form was found to convert by tunneling to the *syn-trans* (**sT**) form with a half-life of 80 min. On the other hand, the photogenerated *anti* conformers (**aC** and **aT**) were found to be stable under the same experimental conditions. Computations grounded on the WKB formalism and using the energy data obtained from B3LYP/6-311++G(3df,3pd) calculations (Figure X.17) were used to rationalize the results and predicted a tunneling half-life for the S–H rotamerization of **sC** to **sT** on the time scale of minutes, in agreement with the experimental observations. On the other hand, the calculations predict the putative **aT**→**aC** tunneling half-life as being of ~2.6 days, but after 18 h of experiment, there was no

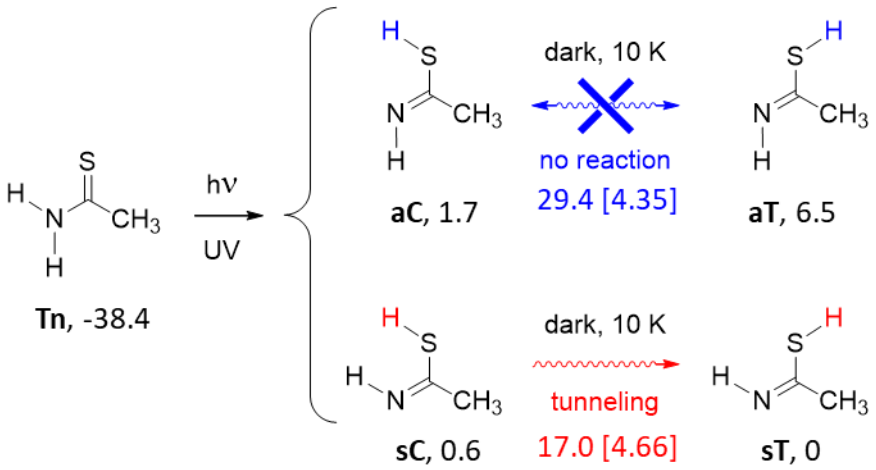

Figure X.17. Isomers of thioacetamide with summary of transformations observed upon UV irradiation of the amino-thione form **Tn** isolated in an argon matrix, and subsequent observed tunneling conformational isomerization (**sC→sT**). The names of the isomers are shown in bold, followed by relative energies with respect to the **sT** thiol isomer. The numbers in blue and red represent the relative energies of the first-order TSs (with respect to **sT**) for the indicated reactions, as well as the barrier widths (in Bohr) along the respective intrinsic reaction paths [in brackets]. Energies of all the stationary points (in kJ mol^{-1}) include the zero-point vibrational energy corrections, computed at the B3LYP/6-311++G(3df,3pd) level of theory. Adapted from Ref. 60 with permission from the PCCP Owner Societies. Copyright 2019.

discernible evidence for such a process (after 18 h, ~18% conversion could be expected). This may be either caused by different interaction of the matrices with the *anti*- and *syn*-imines, which may change the shape of the barriers, or by the different energy gaps between the starting (in the reactant) and final (in the product) vibrational levels, which may favour or disfavour the two processes in a considerably different way, as well as by the assumptions made by the applied tunneling computational method (see Section X.2). This also indicates that imino-thiol systems need further, more advanced, theoretical investigations to be completely understood.

X.7 Bond-breaking/bond-forming H-atom tunneling (H-shifts)

In the previous section we discussed tunneling-induced conformational isomerizations, *i.e.* reactions where the chemical bonding in the reactant and the product has the same topology. In this section we shall discuss other type of tunneling transformations: H-atom shifts, i.e. reactions where chemical bonds are broken, formed, and rearrange from single to double bonds or vice versa. Here we shall skip the tunneling reactions where the structures of the reactant and the product are equivalent by symmetry (such as H-atom shifts in tropolone,[123] malonaldehyde,[124-126] or acetylacetone[124,127]) and will focus on tunneling reactions where the reactant and product are chemically distinct.

Intramolecular hydrogen migrations are frequently associated with reactivity of carbenes. Considerable theoretical and experimental attention has focused on the activation energies, geometrical requirements (orientation) and spin multiplicities involved in such processes. Despite the current interest in carbene reaction dynamics, the tremendously facile nature of intramolecular hydrogen shifts in these species makes direct experimental studies at normal conditions difficult. However, generation, stabilization, and spectroscopic observation of carbenes as well as observation of their rearrangements under cryogenic conditions, make low-temperature techniques very attractive for such kind of studies.[128,129] Early reports, by Chapman[130] and Platz,[131] on application of cryogenic techniques for studies of carbenes, are dated forty years back. Starting from those early works, the carbene intermediates were generated in matrices photochemically from diazo compounds. This way of generation of carbenes is widely used up to date. Here we shall provide some paradigmatic examples involving carbenes.

In 1987, McMahon and Chapman reported on an intramolecular [1,4]-hydrogen shift in a matrix-isolated carbene, which was observed directly by IR and UV spectroscopy.[132] Triplet *o*-tolylmethylene ^{3}**2a** decayed to singlet *o*-xylylene **3a** in an Ar matrix at 4.6 K (Figure X.18). The small temperature dependence and non-Arrhenius behaviour of the decay rate implicated a tunneling mechanism.[132] The reaction was blocked by H/D substitution as expected for a tunneling reaction.

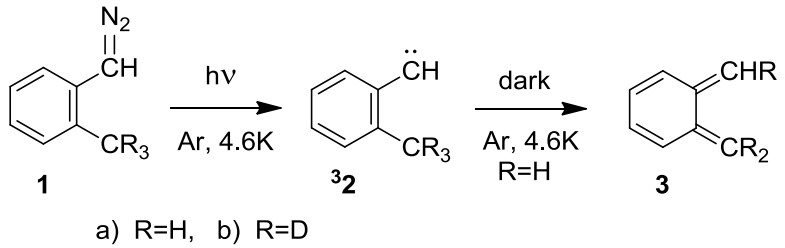

Figure X.18. Tunneling decay of triplet *o*-tolylmethylene ^{3}**2a** to singlet *o*-xylylene **3a**, reported in Reference 132. The deuterated analogue ^{3}**2b** is thermally stable in argon at 19 K and in xenon at 59 K.[132]

In contrast, and as example of exception, triplet 1-phenylethylidene ^{3}**5** is thermally stable in argon or xenon matrices at 10 K (Figure X.19). Warming ^{3}**5** to 65 K in a xenon matrix produced styrene **6**, via an intramolecular [1,2] hydrogen shift. Thermal rearrangement of triplet ^{3}**5a** to styrene **6a** likely occurs upon thermal population of the first excited singlet state of **5** at 65 K. The carbene ^{3}**5** disappearance was observed directly by IR spectroscopy[132] and followed a first order kinetics. This allowed estimating an upper limit of *ca*. 19.7 kJ mol^{-1} for the singlet-triplet energy gap in **5a**.[132] Such a relatively small singlet-triplet energy gap is characteristic of majority of carbenes.

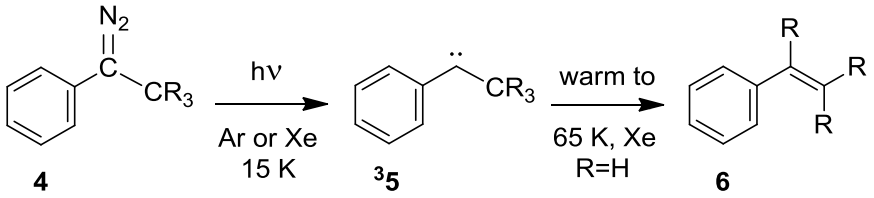

Figure X.19. Triplet carbene 1-phenylethylidene ^{3}**5** is thermally stable in argon or xenon matrices at 10 K. Warming the sample to 65 K in a xenon matrix produces styrene **6**. See Reference 132 for details.

Nitrenes are typically generated in matrices from azide precursors, by photochemical elimination of molecular nitrogen from the N_3 group. One might expect nitrenes to display reactivity similar to their isoelectronic carbene analogues. This has not been true in the systems studied thus far.

Platz et al. observed both triplet nitrene ^{3}**8** and triplet biradical ^{3}**9** upon photolysis of 1-azido-8-methylnaphthalene **7** (Figure X.20).[133,134] Nitrene ^{3}**8** does not produce biradical ^{3}**9** either thermally or photochemically. At 77 K the nitrene ESR spectrum did not interconvert into that of the biradical; both species were indefinitely stable at 77 K,[133,134] and the H-atom abstraction by the nitrene centre did not occur.

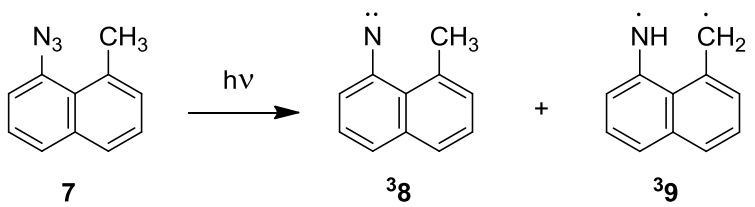

Figure X.20. Photolysis of azide **7** in 2-methyltetrahydrofuran glass at 77 K produces electron spin resonance (ESR) absorptions characteristic of randomly oriented triplet states and are assigned to triplet 1-methyl-8-nitrenonaphthalene ^{3}**8** and triplet biradical 1-imino-8-naphthoquinomethane ^{3}**9**. See Reference 134 for details.

The lack of reactivity of triplet nitrenes toward H-abstraction, even for intramolecular reactions, contrasts with the reactivity of triplet carbenes.[135] This unique behaviour has been interpreted as a result of thermodynamic and electronic factors. Triplet nitrenes are ~165 kJ mol^{-1} more stable than the comparably substituted triplet carbenes.[136] Moreover, the singlet-triplet gap ($\Delta E_{S\text{-}T}$) in nitrenes is generally much larger than in carbenes. The $\Delta E_{S\text{-}T}$ in phenylnitrenes is ~75 kJ mol^{-1} and, therefore, the intersystem crossing (ISC) in phenylnitrenes to their triplet ground-state is often considered irreversible. In phenylcarbenes $\Delta E_{S\text{-}T}$ is less than 20 kJ mol^{-1},[137,138] and consequently the triplet ground-state phenylcarbenes can serve as a reservoir for the highly reactive singlet phenylcarbene.

Recently, we have succeeded in the observation of a first intramolecular H-abstraction reaction in a nitrene.[54] Triplet 2-formyl phenylnitrene **10-*h*** (Figure X.21) was generated by photolysis of 2-formyl phenylazide isolated in Ar, Kr, and Xe matrices. The identity of **10-*h*** was confirmed by IR, UV-vis, and EPR spectroscopies. Upon generation, the triplet nitrene spontaneously rearranged at 10 K in the dark to singlet 6-imino-2,4-cyclohexadien-1-ketene **11-*h*** on the time scale of several hours. This was the first direct evidence of a tunneling reaction in nitrene chemistry.

^{3}**10-*h*** **11-*h***

Figure X.21. Intramolecular tunneling reaction of triplet protium 2-formyl phenylnitrene ^{3}**10-*h*** into imino ketene **11-*h***. See Reference 54 for details.

Several experimental tests were carried out in order to confirm that the transformation of ^{3}**10-*h*** into **11-*h*** was a true tunneling reaction. As expected for tunneling, the reaction is independent of temperature (and in this case also on the matrix material). The calculated barrier for this reaction is above 70 kJ mol^{-1}, which clearly rules out the possibility of an over-the-barrier thermal reaction at 10 K. However, conditions for the occurrence of quantum tunneling are satisfied: the barrier width is rather narrow, no more than 2.1 Å,[54] and the reaction is associated with the movement of the light H atom. Indeed, considering this hypothesis, the H-formyl (^{3}**10-*h***) and D-formyl (^{3}**10-*d***) phenylnitrenes were generated in matrices, and the kinetics of the transformations were studied for both isotopes. The deuterated analogue was found to be indefinitely stable (Figure X.22).

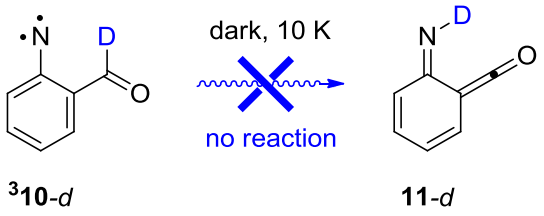

^{3}**10**-*d* **11**-*d*

Figure X.22. Lack of spontaneous decay of triplet deuterated 2-formyl phenylnitrene ^{3}**10-*d***. See Reference 54 for details.

The absence of tunneling in D-formyl phenylnitrene is also confirmed by WKB computations. The life time of ^{3}**10-*d*** was estimated on the order of 150000 years.[54]

Note that a direct transformation of ^{3}**10-*h*** into **11-*h*** is spin-forbidden. We propose that the intramolecular H-shift tunneling initially occurs on the triplet manifold, giving initially an excited triplet state of imino-ketene ^{3}**11**, which is marginally more stable than ^{3}**10**. After the actual H-shift, the singlet electronic ground state **11** is formed by means of intersystem crossing (Figure X.23).

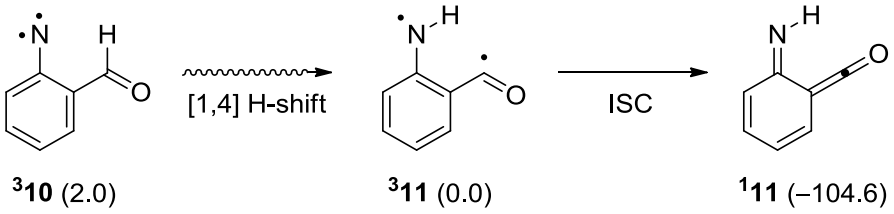

Figure X.23. Mechanism of formation of singlet imino-ketene **11** from triplet nitrene ^{3}**10**, *via* triplet biradical ^{3}**11**. Numbers in parentheses show relative electronic energies, in kJ mol^{-1}, computed at the B3LYP/6-311++G(d,p) level of theory. ISC stands for intersystem crossing. See Reference 54 for details.

Interestingly, Fisher and Michl were able to observe external and internal heavy atom effects, leading to an increased rate of a spin-forbidden proton tunneling reaction. They studied the rearrangement of the 1,3-perinaphthadiyl triplet biradical ^{3}**12** generated by UV-irradiation of cyclopropane **14**. It was found that biradical ^{3}**12** decays to singlet phenalene ^{1}**13** and that the reaction below 100 K proceeds at a temperature-independent rate.[139] This was attributed to quantum mechanical tunneling (by [2,1]-hydrogen shift) from the triplet ground state of ^{3}**12** to the singlet ground state of ^{1}**13** (Figure X.24). The support for a tunneling mechanism also was obtained from a deuterium kinetic isotope effect of 1300.[139]

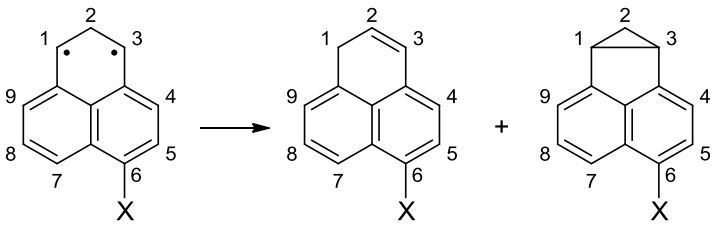

Figure X.24. Tunneling in 1,3-perinaphthadiyl triplet biradical (^{3}**12** and ^{3}**15**) to singlet phenalene. See Reference 139 for details.

Direct evidence of the spin-forbidden nature of the rate-determining tunneling step was obtained by varying the matrix host.[139] The tunneling reaction rate increased by a factor of 10 by going from argon to xenon matrix. Fisher and Michl claimed that an external heavy-atom effect on the tunneling rate for a ground state process had not been observed till then,[139] but mentioned such effects to be well known[140] "to enhance the rate of intersystem crossing from an excited triplet state T_1 to the singlet ground state S_0". An internal heavy-atom effect on the hydrogen-shift reaction was also observed upon introducing a bromine substituent at position 6 (Figure X.24). Fisher and Michl concluded that "the observation of external and internal heavy-atom effects on the temperature-independent rate of tunneling from ^{3}**12** to ^{1}**13** and from ^{3}**15** to ^{1}**16** provided conclusive evidence for its spin-forbidden nature".[139]

Two decades after reports of McMahon and Chapman,[132] and Fisher and Michl,[139] studies on tunneling reactions involving H-atom migration in carbenes gained a considerable renewed attention when Schreiner and co-authors generated and captured methylhydroxycarbene in noble gas matrices at temperatures of around 10 K (reported in 2011).[28] The potential energy surface around methylhydroxycarbene was characterized computationally and large activation enthalpies (over 90 kJ mol^{-1}) were found for two putative [1,2] H atom shifts leading to either acetaldehyde or vinyl alcohol (Figure X.25).

With such high barriers, and under cryogenic conditions, methylhydroxycarbene should not react at all. Still, a first-order reaction consuming methylhydroxycarbene, with a half-life of about 1 h was observed, a transformation that was found to be largely temperature independent.[28] That finding, and the fact that the OD-deuterated methylhydroxycarbene was stable, had led to the conclusion that the reaction exclusively occurred *via* the tunneling mechanism. Among the two possible [1,2]

H-shifts, the reaction in the dark proceeded exclusively to acetaldehyde. This was the first experimental demonstration of the principle of tunneling control, whereby the reaction proceeded only to a product with a higher tunneling probability, albeit facing a higher (but narrower) barrier (Figure X.25).[28]

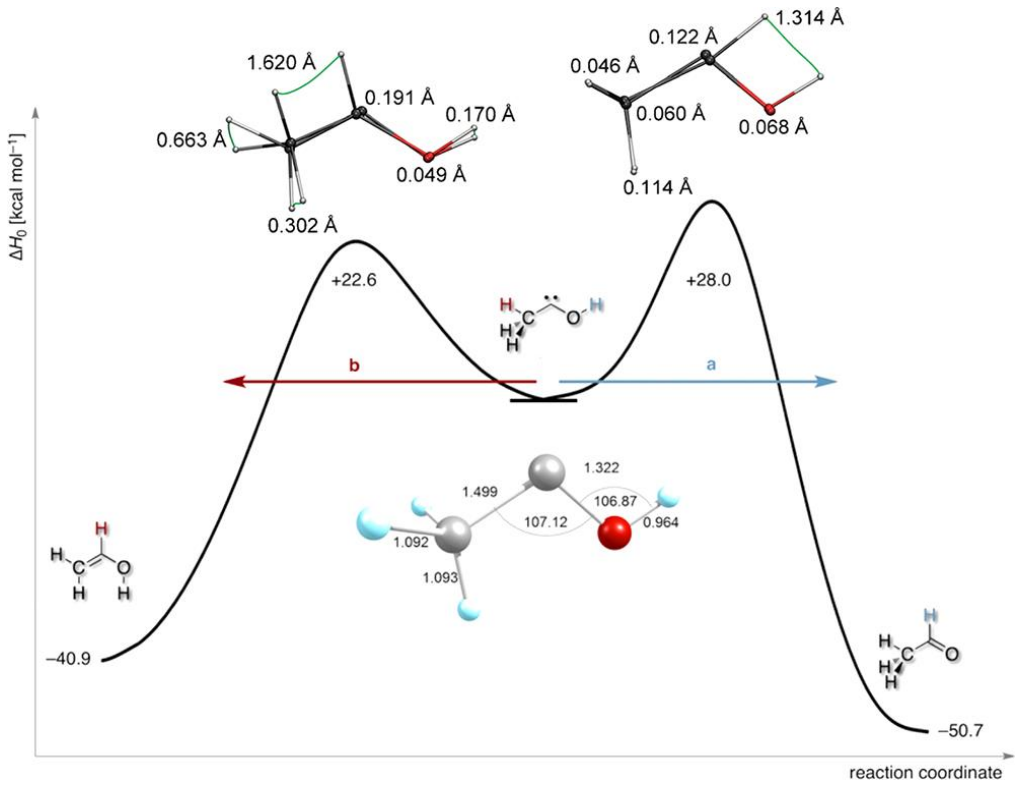

Figure X.25. Computed potential energy surface of methylhydroxycarbene (*middle*: carbon = grey, oxygen = red, hydrogens = light blue) and tunneling paths **a** and **b** to the thermodynamic product acetaldehyde (*right*) or the kinetic product vinyl alcohol (*left*). The paths are intrinsic reaction coordinates that depict the proper heights and widths of the barriers for a fair visual assessment of the potential reactivity. Focal point energies are extrapolated to fully account for electron correlation and an infinitely large basis set using AECCSD(T)/cc-pCVQZ geometries. Reprinted from Ref. 19 with permission from the American Chemical Society. Copyright 2017.

The study on tunneling in methylhydroxycarbene was followed by preparation and experimental characterization of a series of other long-elusive hydroxycarbenes (Figure X.26). Schreiner *et al.* found tunneling control[15] to prevail also for *tert*-butyl-, phenyl-, cyclopropyl-, and trifluoromethylhydroxycarbene by giving the thermodynamic products from [1,2] H-shift tunneling reactions of large but narrow barriers similar to the depiction of Figure X.26. The tunneling half-lives correlate well with the stereoelectronic properties of the R group and depend on the absolute barrier height (with very similar overall shapes).[15] Also, when the carbene carbon atom was stabilized by another π-donor heteroatom (N or O), tunneling was not observable at laboratory time scales.[15]

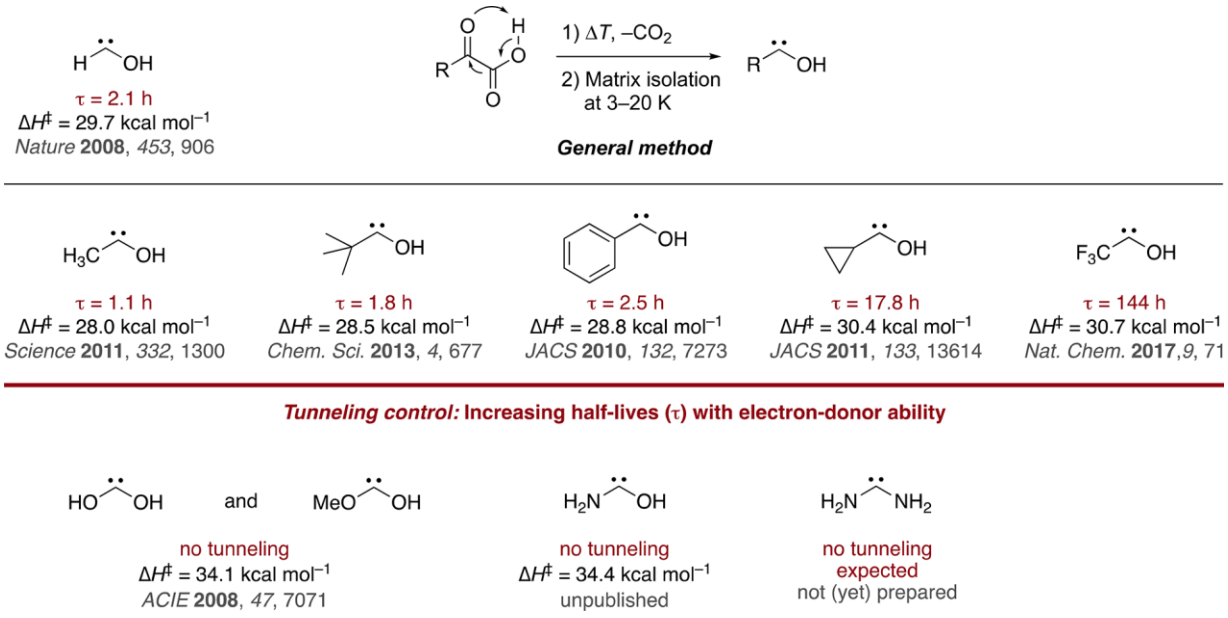

Figure X.26. Family of hydroxycarbenes with HCOH as the parent species (*top left*)[141] and the general way of preparation through thermal extrusion of CO_2 from α-ketocarboxylic acids. *Middle*: tunneling half-lives τ and [1,2] H-shift barriers for the associated tunneling process computed at the coupled cluster level of theory with at least triple-ζ basis sets.[28,142-145] *Bottom*: related diheteroatom-substituted carbenes that do not show tunneling.[146] Reprinted from Ref. 19 with permission from the American Chemical Society. Copyright 2017.

The research on H-atom tunneling in carbenes actively continues.[147,148] Very recently, a new member was added to the family of hydroxycarbenes. Eckhardt, Erb and Schreiner reported the gas-phase preparation of cyanohydroxycarbene by high-vacuum flash pyrolysis of ethyl 2-cyano-2-oxoacetate and subsequent trapping of the pyrolysate in an inert argon matrix at 3 K (Figure X.27).[149] After a few seconds of irradiation of the matrix with green light, singlet *trans*-cyanohydroxycarbene **17t** rearranges to its *cis*-conformer **17c**.

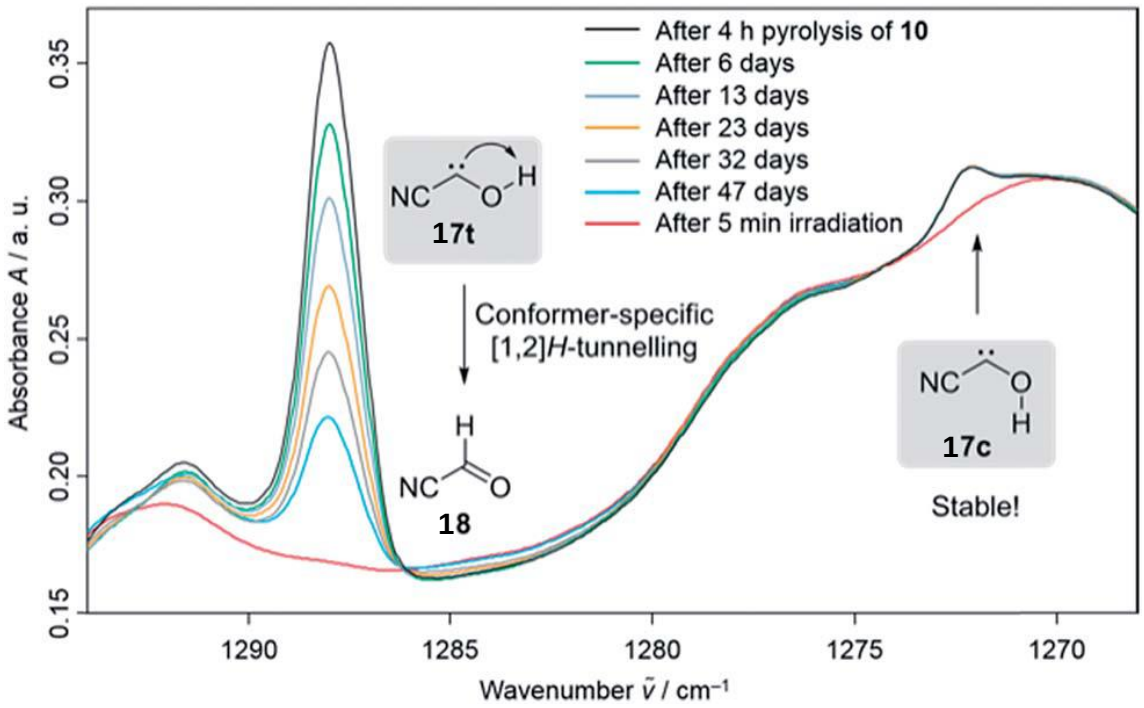

Figure X.27. Conformer-specific [1,2] H-tunneling of *trans*-cyanohydroxy-carbene (**17t**) with a tunneling half-life of 23.5 days over a time period of 47 days monitored by the signal decay at 1288 cm^{-1}. The amount of the *cis*-conformer **17c** remained unchanged over the same period (band at 1272 cm^{-1}). After 5 min irradiation of the matrix with a light of 520 nm, both carbene signals are completely depleted (red spectrum). Adapted from Ref. 149 with permission from The Royal Society of Chemistry.

Cis- and *trans*-cyanohydroxycarbene were characterized by IR and UV-vis spectroscopy. *Trans*-cyanohydroxycarbene **17t** undergoes a conformer-specific [1,2] H-tunneling reaction through a 139.3 kJ mol^{-1} barrier (the highest penetrated barrier of all H-tunneling reactions observed to date) to cyanoformaldehyde **18** with a half-life of 23.5 days; this is the longest half-life reported for an H tunneling process to date. During the tunneling reaction the *cis*-conformer **17c** remains unchanged over the same period of time (see Figure X.27).[149]

One of interesting questions is: what if the oxygen atom of the hydroxycarbene would be substituted by either a sulphur or a selenium atom? Do the mercaptocarbene (H-C-S-H) and selenocarbene (H-C-Se-H) congeners of hydroxycarbene (H-C-O-H) also undergo [1,2] H-tunneling? Schreiner and co-authors addressed this question theoretically.[150] Comparison of the computed intrinsic reaction paths of the reactions *trans*-HCXH to H_2CX (X = O, S, Se) indicated that the energetic characteristics of the paths are very similar (126-139 kJ mol^{-1}). For the three [1,2] H-shift reactions investigated, the barrier is considerably narrower for the parent [H,H,C,O] system than those for [H,H,C,S] and [H,H,C,Se]. It was then concluded that the tunneling half-lives for the X = S and X = Se unimolecular isomerization reactions are expected to be much longer than that for the *trans* HCOH $\rightarrow$ H_2CO reaction. This means that unlike for the parent hydroxymethylene (HCOH), at the low temperatures of matrix isolation experiments no tunneling will be observable for the *trans*-HCSH and *trans*-HCSeH systems. The most intriguing fact is that, despite numerous experimental attempts to synthesize *trans*-HCSH or *trans*-HCSeH *via* routes similar to those that resulted in the formation of the parent hydroxymethylene, these [H,H,C,S] thiol or [H,H,C,Se] selenol isomers have thus far remained inaccessible under matrix isolation conditions.

There are, however, reports on trapping thiol (SH) and selenol (SeH) compounds under matrix isolation conditions and experimental observation of the respective tunneling isomerizations into their thione (C=S) or selenone (C=Se) congeners. Rostkowska and co-authors trapped the amino-thione form of thiourea in argon matrices (Figure X.28) and, by using UV-irradiation (λ > 270 nm), they generated *in situ* two imino-thiol isomers (**20tl** and **21tl**).[151] They observed that the *anti*-imino-thiol **21tl** isomer converted back to the **19tn** form at 10 K, and in the dark, with a time constant of 52 hours (Figure X.28). The molecules in the *syn*-imino-thiol **20tl** conformation remained unchanged. The authors concluded that "the only possible mechanism of the ground-state thiol → thione transformation at low temperature is hydrogen tunneling through the very high energy barrier (108 kJ mol^{-1}, as calculated at the MP2/6-31++G(d,p) level)".[151]

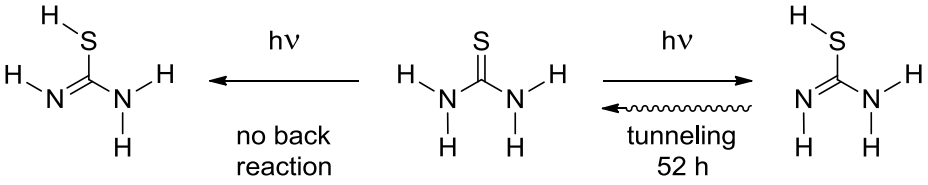

Figure X.28. Photochemical generation of imino-thiol forms (**20** and **21**) of thiourea **19** isolated in an Ar matrix and spontaneous thiol → thione tunneling for one of the imino-thiol isomers. See References 151 and 152 for details.

15 years later, the same group of authors reinvestigated the reactions for the thiourea molecules isolated in Ar, Ne, n-H_2 and n-D_2 matrices at 3.5 K.[152] The less stable thiol form of the compound was photochemically generated by UV irradiation of the matrix, and after that, a spontaneous thiol → thione conversion was studied as a function of matrix material or matrix temperature. The authors did not find any drastic dependence of the tunneling rate either on the matrix environment (measured

time constants between 52 and 94 hours in four different hosts), or on the matrix temperature (between 3.5 and 15 K in Ar).[152]

Rostkowska *et al.* have also studied H-atom transfer processes for selenourea isolated in Ar matrices.[153] Initially, the monomers of selenourea adopt exclusively the selenone tautomeric form **22** (Figure X.29). UV irradiation of the matrix-isolated compound led to generation of the selenol tautomer **23**. For the matrix kept at 10 K and in darkness, an H-atom tunneling reaction transforming the photoproduced selenol *anti* form **23a** back into the initial selenone tautomer **22** was observed[153] (Figure X.29). Interestingly, the selenol → selenone tunneling reaction in selenourea was considerably quicker (16 h)[153] than the analogous thiol → thione tunneling in thiourea (52 h)[151] despite the computed barriers are rather similar: 95 kJ mol^{-1} [MP2/6-311++G(2d,p)][153] and 108 kJ mol^{-1} [MP2/6-31++G(d,p)].[151] The difference in observed tunneling rates must be related with the barrier widths which were not reported.

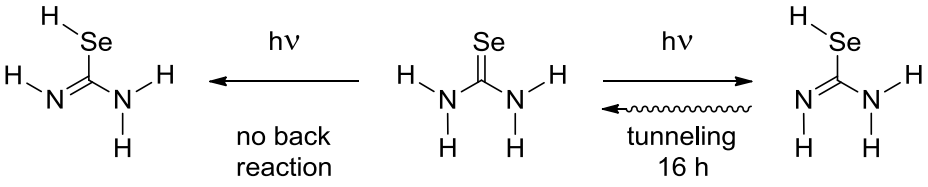

Figure X.29. Photochemical generation of imino-selenol forms of selenourea isolated in an Ar matrix and spontaneous selenol → selenone tunneling for one of the imino-selenol isomers. See Reference 153 for details.

The experimental observations of tunneling in imino-thiol and imino-selenol compounds means in the first place that these high-energy forms can be successfully generated. On the other hand, Schreiner and co-authors suggest that part of the reason for not being able to synthesize in matrices carbene-thiol (and

carbene-selenol) isomers is that *trans*-HCSH is not a true carbene but is better represented as an ylide with a negatively charged carbon atom and a positively charged sulphur.[150]

The thiol → thione proton tunneling in thiourea (and selenourea) can also be compared with structurally similar molecule of thioacetamide. Similarly to thiourea, matrix-isolated molecules of thioacetamide initially exist exclusively as amino-thione tautomer. The imino-thiol isomer can be generated in cryogenic matrices by means of UV-irradiation (see Figure X.30).[60,154]

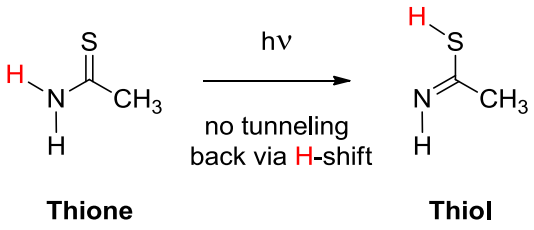

Figure X.30. UV-induced generation of imino-thiol tautomer of thioacetamide. The imino-thiol can exist in four isomeric structures, but only the "tunneling-ready" isomer is shown in the Figure. Reverse thiol → thione proton tunneling in thioacetamide was not observed. See References 60 and 154 for details.

The lack of thiol → thione tunneling transformation in thioacetamide is consistent with its relatively high barrier. Calculated at the MP2/6-31++G(d,p) level, it equals to 123 kJ mol^{-1}.[154] This is higher than the MP2-computed barriers for thiol → thione transformation in thiourea (108 kJ mol^{-1})[151] or selenourea (95 kJ mol^{-1}).[153]

The barrier for thiol → thione proton tunneling in thioacetamide was also calculated at the B3LYP/6-311++G(3df,3pd) level, and the obtained value was 108.5 kJ mol^{-1}.[60] Considering this barrier height, and also the barrier width (1.29 Å) of the calculated intrinsic reaction path, a tunneling half-life of 100 days (8.63 × 10^6 s) for thiol →

thione isomerization was computed using the WKB approximation.[60] This would imply a tunneling reaction too slow to be observed within the time limits achievable in our experiments.

Carbenes are among the few metal-free molecules that are able to activate molecular hydrogen. The reactivity patterns of carbenes depend on the substituents at the carbene centre. Closed-shell singlet carbenes can be described as 1,1-zwitterions, bearing both nucleophilic and electrophilic regions at the carbene center. Singlet carbenes insert in concerted reactions with considerable activation barriers, and are thus poorly reactive towards H_2 at cryogenic temperatures. In contrast, triplet carbenes exhibit radical-like reactivity, such as atom abstractions.[155] They quickly yield radical pairs that rapidly undergo secondary reactions (Figure X.31).[156] These properties of carbenes can be used for activation of molecular hydrogen, a topic actively studied by Sander et al.[156] A paradigm in carbene chemistry is that reactions of carbenes are spin specific and occur from equilibrated spin states, depending on the temperature.

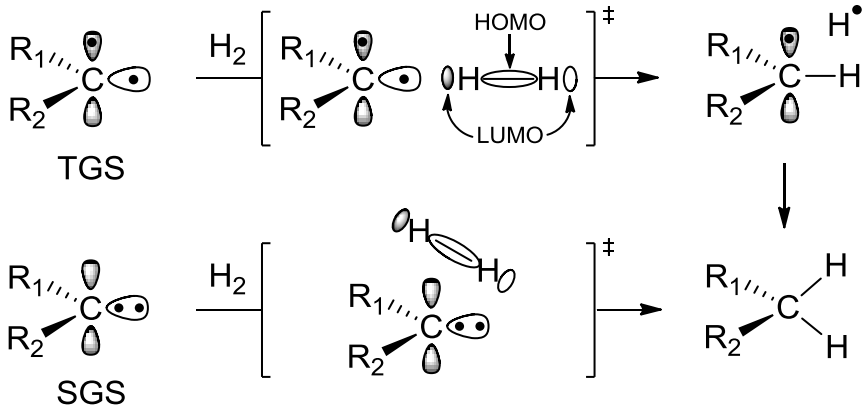

Figure X.31. Reactions of singlet ground state (SGS) and triplet ground state (TGS) carbenes with molecular hydrogen. See Reference 156 for details.

4-Oxocyclohexa-2,5-dienylidene **24** has a triplet ground state (TGS) carbene that is highly reactive toward solid H_2, HD, and D_2 at 3 K. Sander *et al.* investigated the mechanism of the insertion of this carbene into dihydrogen by IR and EPR spectroscopy and by kinetic studies.[157] The hydrogenation showed a very large kinetic isotope effect and remarkable isotope selectivity, as could be expected for a tunneling reaction. H or D atoms were observed as products of the reaction with H_2 or D_2, respectively, whereas HD produces exclusively D atoms (Figure X.32).[157] The experiments of Sander *et al.*, therefore, provide clear evidence for both hydrogen tunneling and the rare deuterium tunneling in an intermolecular reaction.[157]

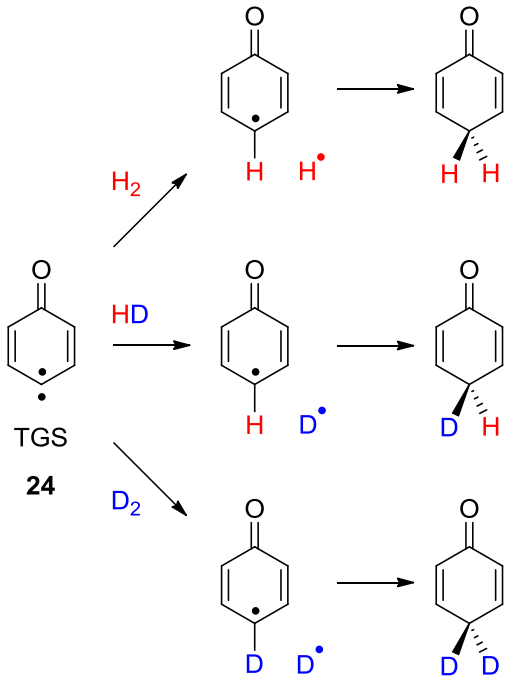

Figure X.32. Reaction of 4-oxocyclohexa-2,5-dienylidene **24**, which is a carbene characterized by triplet ground state (TGS), with H_2, HD, and D_2. See Reference 157 for details.

The activation barrier for the reaction of 4-oxocyclohexa-2,5-dienylidene **24** (Figure X.32) with hydrogen was calculated to be 22.6 kJ mol^{-1}, which is higher than the

thermal energy available at 30 K.[157] Similar barriers were found for the other triplet ground state carbenes, such as cyclopentadienylidene studied by Zuev and Sheridan.[158] Therefore, these carbenes should not react thermally with hydrogen at very low temperatures, which suggests that the reaction rates are governed by quantum chemical tunneling. For tunneling reactions, large kinetic isotope effects (KIE) are expected, and indeed, with D_2 no reaction was observed by Sander et al., under conditions in which H_2 rapidly reacts.[157] Zuev and Sheridan concluded that the *"most likely pathway is single H abstraction by tunneling to give a triplet radical pair, which then combines following intersystem crossing"*.[158]

Recently, Henkel *et al.* reported that 1-azulenylcarbene **25** has a singlet ground state (SGS), in contrast to most other arylcarbenes that show triplet ground states.[159] Carbene **25** can be generated by photolysis of 1-azulenyldiazomethane **26** (Figure X.33), but even at 3 K it is kinetically unstable and quickly rearranges to the strained allene **27** through QMT.[159] The tunneling reaction can be completely blocked by deuteration at position 8 in the seven-membered ring (Figure X.33). Upon studies in neat noble gas matrices,[159] Henkel and Sander reported their investigations on the reaction of singlet carbene **25** with molecular hydrogen.[160] To suppress the rearrangement of **25** through QMT, only the dideuterated isotopomer **d_2-25** (Figure X.34) was used in their experiments.[160] It was demonstrated that 1-azulenylcarbene **25** with a singlet ground state readily inserts into H_2, and slowly into D_2, proving that QMT governs the insertion into both H_2 and D_2 (Figure X.34). This was the first example showing that QMT can also be important for singlet carbenes inserting into dihydrogen.[160]

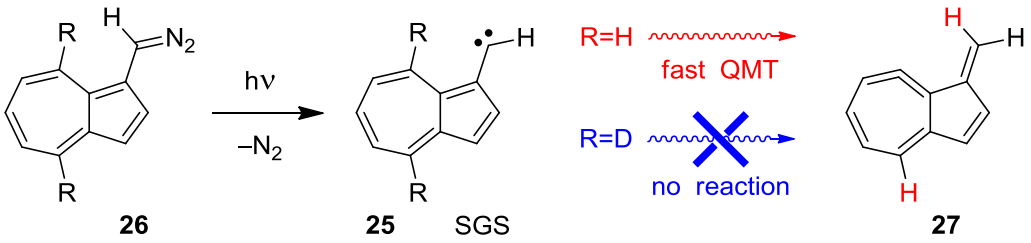

Figure X.33. Photochemical generation and quantum mechanical tunneling (QMT) rearrangement of 1-azulenylcarbene **25**, which is a carbene characterized by a singlet ground state (SGS). QMT occurs only for R=H. See Ref. 159 for details.

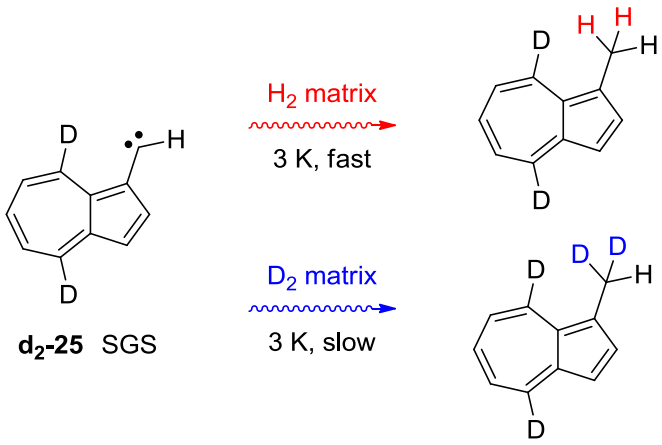

Figure X.34. Reactivity of singlet dideuterated 1-azulenylcarbene **d_2-25** with hydrogen and deuterium in neat H_2 and D_2 matrices. See Ref. 160 for details.

As a culmination of their research on activation of molecular hydrogen, Sander *et al.* have very recently discovered a magnetically bistable carbene (3-Methoxy-9-fluorenylidene **28**), and reported on its photochemically-induced conformational spin switching and spin-selective hydrogenation.[161] 3-Methoxy-9-fluorenylidene **28** was generated in cryogenic matrices both in its lowest energy singlet and triplet states, and the ratio of these states was shifted by selective irradiation (Figure X.35).[161] The interconversion of the nearly degenerate spin states was achieved by a conformational change of the methoxy group: “up” position results in the singlet state

and switching into the “down” position yields the triplet state (Figure X.36).[161] The spin control *via* a remote functional group makes this carbene unique for the study of spin-specific reactions, which is demonstrated for the hydrogenation reaction. Sander et al. suggest that the control of the spin states opens the path to tuning selectivity in chemical reactions and to developing novel magnetically switchable materials.[161]

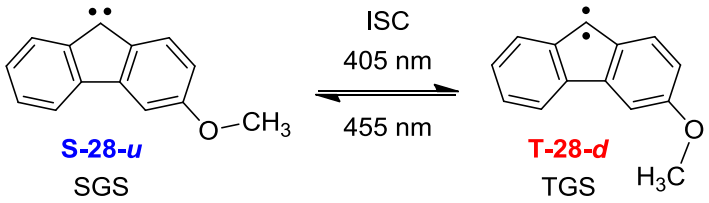

Figure X.35. The unique spin switching of carbene **28** induced by conformational change of a remote functional group. ISC: intersystem crossing; SGS: singlet ground state, TGS: triplet ground state. Suffixes “u” and “d” designate “up” and “down” conformations of the methoxy group. See Ref. 161 for details.

The experiments clearly demonstrated that the insertion of carbene **28** into D_2 is both spin and conformation specific. Only triplet carbene **T-28-d** (Figure X.36) reacts with D_2 to produce the “down” fluorene conformer exclusively, whereas the singlet carbene **S-28-u** is indefinitely stable in solid deuterium. Conformational spin switching by a remote functional group, a new phenomenon discovered by Sander et al., could be utilized beyond tracing spin states in mechanistic studies. They propose that “the introduction of a bulkier or conformationally restricted ether, amino, or similar groups should allow to manipulate spin states, and thus the magnetic properties, of molecular materials. Such switchable molecular materials have potential applications in information recording”.[161]

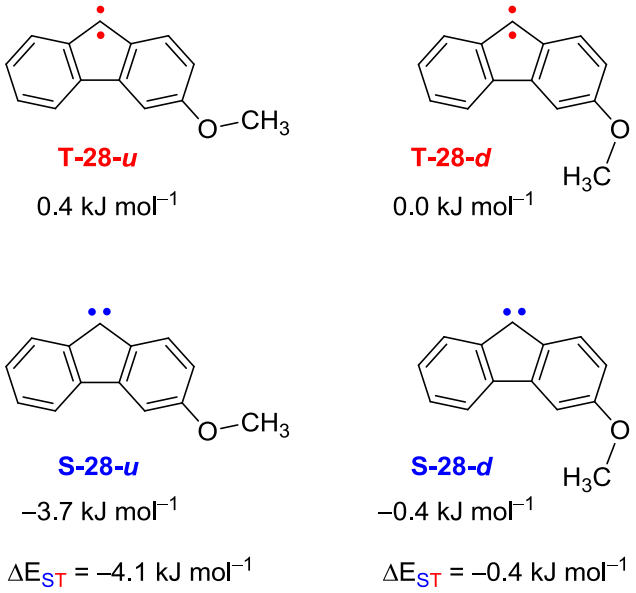

Figure X.36. Two conformers were considered with respect to the orientation of the methoxy group in singlet **S-28** and triplet **T-28**, denoted as "up" (**u**) and "down" (**d**) conformers. Geometries were optimized at the B3LYP-D3/def2-TZVP level and energies were refined by single point CCSD(T)/cc-pVTZ calculations. See Ref. 161 for details.

Finally, Haupa *et al.* have recently demonstrated that hydrogen abstraction/addition tunneling reactions elucidate the interstellar H_2NCHO/HNCO ratio and explain the H_2 formation.[162] Interstellar observations show a strong correlation between the abundance of formamide (H_2NCHO) and isocyanic acid (HNCO), indicating that they are likely to be chemically related, but no experiment or theory could explain this correlation satisfactorily.[162]

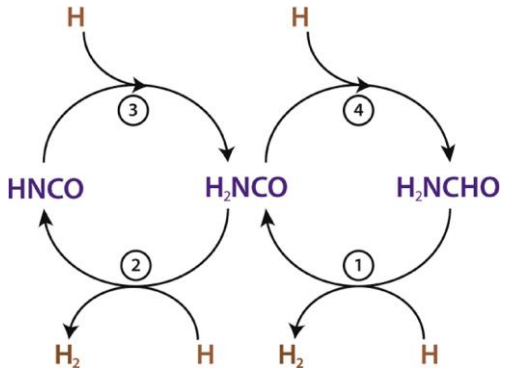

Figure X.37. Dual-cyclic mechanism of H-abstraction and H-addition reactions connecting H_2NCHO, H_2NCO, and HNCO. Reprinted from Ref. 162 with permission from the American Chemical Society. Copyright 2019.

Haupa *et al.* have studied reactions of formamide in a *p*-H_2 matrix and identified production of H_2NCO and HNCO from hydrogen-abstraction reactions.[162] Haupa *et al.* observed temporal profiles of H_2NCHO, H_2NCO, HNCO, and their deuterium isotopologues, and showed that a dual-cycle consisting of hydrogen abstraction and hydrogen addition (Figure X.37) can satisfactorily explain the quasi-equilibrium between H_2NCHO and HNCO and explain other previous experimental results.[162] In the proposed mechanism, it was assumed that the H atoms produced in the reaction cycle can move efficiently through the lattice on continuously breaking and formation of neighbouring H−H bonds via quantum tunneling.[162]

X.8 Heavy-Atom Tunneling

As shown in the previous sections of this chapter**,** H-atom tunneling is a common phenomenon. Its relevance in chemistry has been stressed long ago, in particular when Bell published his seminal theoretical paper demonstrating the need to consider tunneling for a correct description of reactions involving the motion of a

hydrogen atom or a proton.[3] Interestingly enough, he also predicted that under normal conditions heavier atoms should behave classically. Because, as discussed before, tunneling probabilities decrease exponentially with the square root of the moving mass, tunneling of a carbon atom, 12 times heavier than hydrogen, can indeed be predicted to be much less likely. According to the expectations, for almost half-century, Bell's claim was practically unchallenged. The paradigm only shifted when experimentalists published the first examples of heavy-atom tunneling in the mid-70's/80's. Nonetheless, forty years after the first examples being reported, the number of experimental observations of heavy-atom tunneling reactions is still small. Considering that a hydrogen atom can tunnel across a barrier of around 1 Å, a carbon atom can be expected to tunnel through a barrier with a width of $12^{-1/2} \approx 0.3$ Å with the same probability (assuming a barrier of similar height and shape).[163] Such very narrow barriers are expected to occur only in processes involving very reactive species or, as Kozuch *et al.* highligthed,[163] in strongly exothermic reactions or some symmetrical isothermic transformations. Indeed, these conditions have been matched in almost all of the heavy-atom tunneling reactions observed so far.

One of the first experimental evidence of heavy-atom tunneling was reported by Buchwalter and Closs in 1975,[164] namely for the ring-closure of triplet 1,3-cyclopentanediyl **30** to bicyclopentane **31** (Figure X.38). The triplet 1,3-diradical ^{3}**30** was generated by UV irradiation of a matrix-isolated diazo precursor **29** and characterized by EPR spectroscopy. The EPR signals assigned to ^{3}**30** were found to diminish in intensity with a half-life of 30 min, and the reaction rate was observed to be essentially the same between 1.3 and 20 K. Based on this temperature independence, it was suggested that the reaction takes place by tunneling.[164,165]

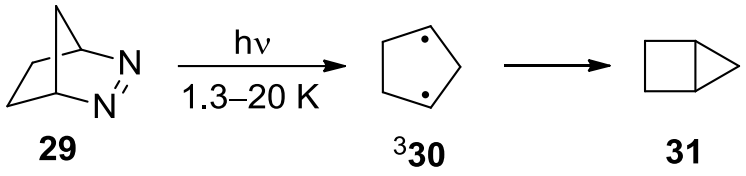

Figure X.38. Ring-closure of triplet 1,3-cyclopentanediyl ^{3}**30** to bicyclopentane **31**.

Additional evidence of heavy-atom tunneling in the ring-closure of triplet 1,3-diradicals was reported later by Dougherty *et al.* (Figure X.39).[50] They observed that the EPR signals of methyl and ethyl substituted triplet 1,3-cyclobutanediyls ^{3}**32** decay at temperatures as low as 3.8 K. The kinetic treatment of the measured rate constants between 4 and 20 K gave non-linear Arrhenius plots. These observations clearly suggest the occurrence of tunneling.

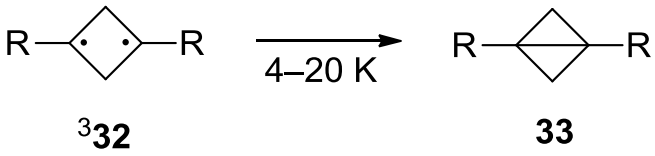

Figure X.39. Ring-closure of triplet 1,3-cyclobutanediyls ^{3}**32** to bicyclobutanes **33**.

In their studies, Closs, Dougherty and coworkers noted that the observed decay kinetics were complicated by the existence of a distribution of rate constants resulting from different matrix sites[50,164,165] (see also section X.4). It is also interesting to note that, in both studied cases,[50,164,165] triplet 1,3-diradicals must undergo intersystem crossing (ISC) to form the singlet products. However, it is not yet clear (even today) if tunneling takes place on the triplet surface, to a geometry that then undergoes ISC to the singlet surface, or if tunneling occurs concomitantly with the ISC process.[22]

The studies on the interconversion between valence isomers of cyclobutadiene (Figure X.40) can be considered a milestone among the investigations on heavy-atom tunneling reactivity. About forty years ago, Whitman and Carpenter investigated, using variable temperature NMR spectroscopy, the isomerization rate of cyclobutadiene-1,4-d_2 **34** (selectively generated *in situ* from a precursor) to cyclobutadiene-1,2-d_2 **35**, concomitantly with the rate of trapping **34** and **35** in a cycloaddition reaction.[166] The unexpected negative entropy value found for the isomerization of cyclobutadiene was interpreted as an evidence that the reaction was taking place by carbon tunneling.[166,167] Afterwards, Michl *et al.* reported polarized IR and ^{13}C NMR spectra of cyclobutadiene and its vicinal ^{13}C-dilabeled derivative, photogenerated in rare-gas matrices.[168] Based on the spectroscopic observations, it was determined that the two valence isomers **34** and **35** were rapidly interconverting (at a rate $>10^{-3}$ s^{-1}) in the matrices at 25 K. They concluded that the observed isomerization had to be due to tunneling, since the reaction barrier (estimated as ~40 kJ mol^{-1}) cannot be overcome at the temperatures of the experiments.

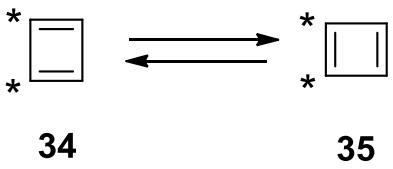

Figure X.40. Valence isomerization between 1,4-labeled-cyclobutadiene **34** and 1,2-labeled-cyclobutadiene **35**.

A recent case of heavy-atom tunneling in an almost symmetrical isothermic reaction was reported by Sander and coworkers (Figure X.41).[169] Interestingly, this experimental work was inspired by an earlier theoretical study carried by Borden *et*

al.,[170] where the authors, using computations performed at the B3LYP/6-31G(d) level within the small-curvature tunneling (SCT) methodology, predicted that the Cope rearrangement of semibullvalene (and some derivatives) should take place by tunneling at cryogenic temperatures. In their article, they recommended to perform experiments on 1,5-dimethylsemibullvalene substituted with one deuterium atom to break symmetry. The presence of the deuterium atom either at position 4 or 2 (corresponding to the isotopomers **36** and **37** in Figure X.41, respectively) leads to an energy difference between the two isomers of ≈ 0.7 kJ mol^{-1}, with **36** being separated by a barrier of *ca.* 23 kJ mol^{-1} from the most stable isotopomer **37**.

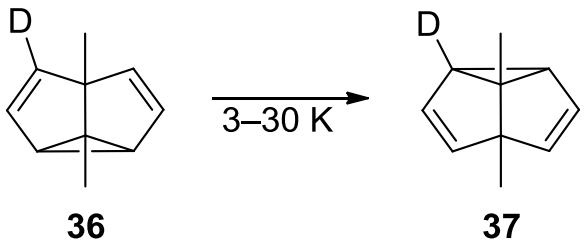

Figure X.41. Cope rearrangement of 1,5-dimethylsemibullvalende-4-d_1 **36** to 1,5-dimethylsemibullvalende-2-d_1 **37.**

In the experiments performed by Sander and coworkers, the room temperature equilibrium mixture (≈ 1:1) of isotopomers **36** and **37** was deposited in a matrix at 3 K and both species characterized by their mid-IR spectrum.[169] Subsequently, the matrix was kept in the dark for several hours. They observed that the intensity of the IR signals assigned to **36** decreased, whereas those due to **37** increased (Figure X.42). Because the barrier between the isotopomers cannot be overcome at the cryogenic temperature used in the experiments, the observed Cope rearrangement from **36** to **37** can only take place by heavy-atom tunneling, thus confirming the theoretical predictions.[170]

The reaction kinetics was also measured as a function of the temperature, although it is complicated by its dispersive character. The rate of the Cope rearrangement in argon matrix was then found to increase only by a factor 3 on increasing the temperature by a factor of 10 (3 to 30 K), providing additional support for the existence of heavy-atom tunneling. The noticed small increase in the rate of the process can be justified by changes in the medium resulting from the matrix softening.

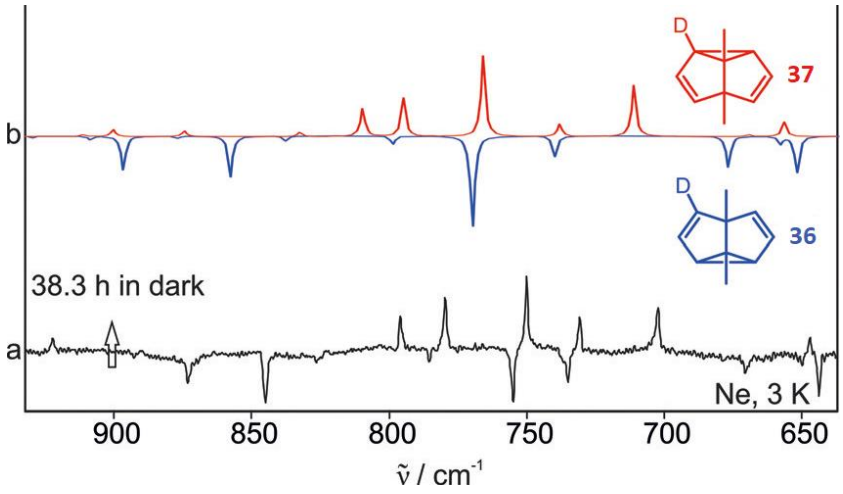

Figure X.42. (a) IR difference spectra showing the Cope rearrangement of **36** to **37** after keeping a neon matrix containing a mixture of **36** and **37** in the dark for 38.3 h at 3 K. (b) Computed B3LYP/6–311G(d,p) IR spectra of **36** (pointing downwards) and **37** (pointing upwards). Adapted from Ref. 169 with permission from John Wiley and Sons. © 2017 Wiley-VCH Verlag GmbH & Co. KGaA, Weinheim.

Two puzzling observations related with the studies reported by Sander and coworkers that still do not have a clear explanation shall be mentioned here: (i) the Cope rearrangement tunneling does not take place in solid xenon nor in the absence of a matrix, whereas in neon, argon, nitrogen, and para-hydrogen the rates were comparable, and (ii) after very long reaction time, the Cope rearrangement tunneling

resulted in a ratio between the isotopomers far from the expectations (*e.g.*, in argon at 5 K: *initial ratio* = 1:1.3; *final ratio* (16.1 h) = 1:1.5, *final ratio expected* = $1:10^{-5}$).

Another example of heavy-atom tunneling reported by Sander's group was the ring-expansion of the fused cyclopropane **38** to triplet carbene ^{3}**24** (Figure X.43). [53,171] Cyclopropene derivative **38** was generated by Vis irradiation of triplet carbene ^{3}**24**, which in turn was obtained in cryogenic matrices by the photolysis of a quinone diazo derivative. It was found that the intensities of the IR bands of **38** decrease in the dark, while those of ^{3}**24** increase. A detailed kinetic study of this transformation showed that the Arrhenius plots between 3 and 20 K are temperature independent (in matrices of several different host gases), clearly indicating that the ring-expansion was taking place through heavy-atom tunneling (Figure X.44).[53] At temperatures above 25 K, the rates increase rapidly (independent of the matrix host), which was interpreted as a result of occurrence of thermally activated tunneling. The different reaction rates observed for different matrix host gases were a consequence of the matrix influence on the barrier width and height. Particularly noticeable was the acceleration at 3 K of the tunneling rates in xenon ($\tau_{1/2} \approx 5$ h) compared to those observed in argon ($\tau_{1/2} \approx 7$ days). Nevertheless, these matrix effects are not yet clearly understood.

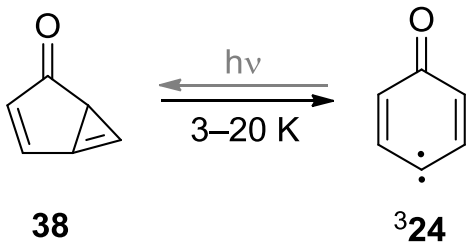

38 ^{3}**24**

Figure X.43. Ring-expansion reaction of 1H-bicyclo[3.1.0]-hexa-3,5-dien-2-one **38** to 4-oxocyclohexa-2,5-dienylidene ^{3}**24**.

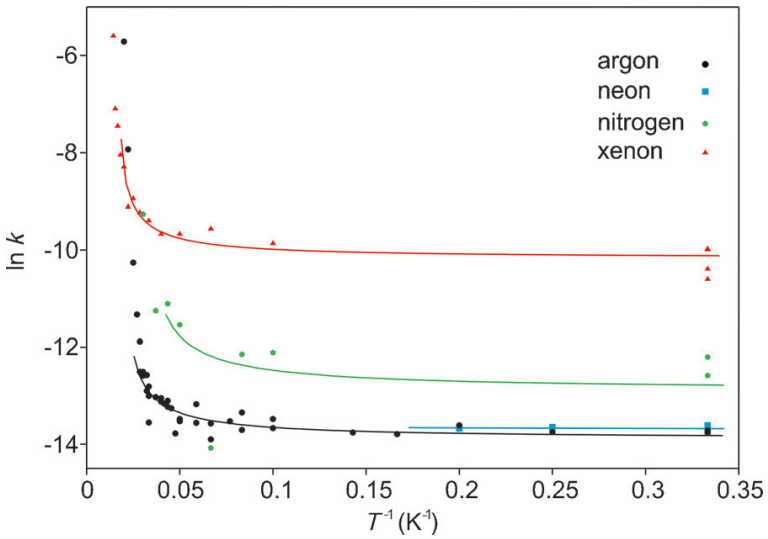

Figure X.44. Arrhenius plots for the ring-expansion of **38** to ^{3}**24** in neon, argon, nitrogen and xenon matrices. Reproduced from Ref. 53 with permission from John Wiley and Sons.

An interesting feature of this ring-expansion reaction is the existence of an ISC step, since cyclopropane **38** has a singlet ground state and carbene **24** has a triplet ground state. Multi-configurational calculations revealed further that carbene **24** has an open-shell singlet state (OSS) as the lowest singlet state, which is energetically more stable (≈16 kJ mol^{-1}) than cyclopropane **38**. Therefore, the proposed mechanism for the formation of triplet carbene ^{3}**24** at cryogenic temperatures involves the ring-expansion of **38** to OSS **24** by heavy-atom tunneling, followed by ISC of OSS **24** to ^{3}**24**. CASPT2 computations were carried out,[53] and the activation energy for the ring-expansion of **38** to OSS **24** was estimated as being 29-33 kJ mol^{-1}. This energy barrier should result in a rate of effectively zero for the over-the-barrier reaction at the used cryogenic temperatures. Then, the rate constants were evaluated using the small-curvature tunneling (SCT) approximation. The performed calculations led to rate constants which were independent of the temperature up to 50 K, thus indicating that the only tunneling contribution to the ring-expansion of **38**

to OSS **24** should originate from the ground vibrational level. The predicted rate of $2 \times 10^{-6} - 2 \times 10^{-8}$ s^{-1} (depending on the basis set used) was found to reasonably agree with the experimental rate of 1.2×10^{-6} s^{-1} measured in an Ar matrix at 3 K.

Two other examples of heavy-atom tunneling involving ring-expansion reactions were reported for benzazirine rearrangement to a cyclic ketenimine: the first, discovered by McMahon's group for the reaction of **39** to **40**,[172] and the second discovered by our group for the reaction of **41** to **42** (Figure X.45).[173]

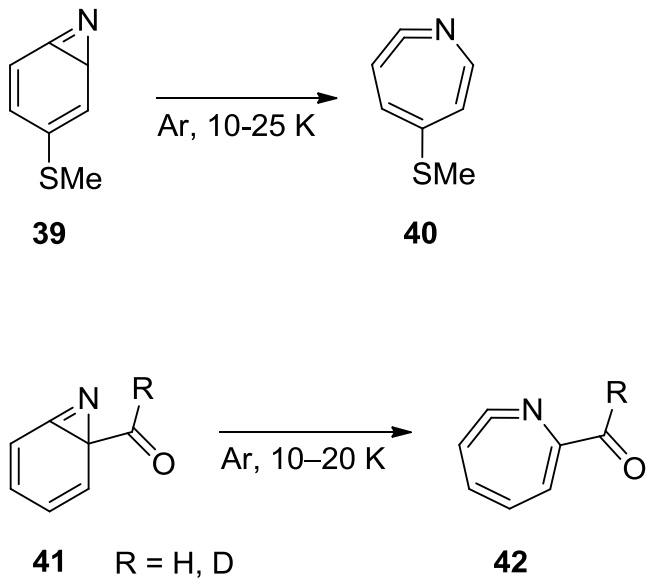

Figure X.45. Ring-expansion reaction of benzazirines **39** and **41** to cyclic ketenimines **40** and **42**, respectively.

The McMahon's group showed that irradiation of 4-methylthiophenylazide in argon matrix with 365 nm light mainly leads to the corresponding arylnitrene.[172] The irradiation of this arylnitrene at 313 or >415 nm leads to its rearrangement to the cyclic ketenimine **40** [ν(C=C=N) = 1889 cm^{-1}], which then slowly converts to benzazirine **39** [ν(C=N) = 1717 cm^{-1}] upon irradiation at >415 nm. They found that ring-expansion of benzazirine **39** to ketenimine **40** takes place spontaneously in the

dark, with a rate constant that shows almost no temperature dependence from 10 K (1.5×10^{-5} s^{-1}) to 25 K (1.8×10^{-5} s^{-1}), which clearly suggests heavy-atom tunneling. B3LYP/6-31G(d) calculations estimated an activation barrier of 14 kJ mol^{-1} for the reaction of **39** to **40**, indicating that it cannot occur as a thermally activated process, because a rate constant to surmount this barrier at 10 K would be around 2.0×10^{-63} s^{-1} (based on the Eyring equation).

When the methylthio moiety was replaced by a methoxy group, the corresponding benzazirine was found stable under the low temperature matrix conditions; no evidence for tunneling was observed. The different behavior of the two compounds was rationalized in terms of the height and width of the associated energy barriers, which were found to be greater for the methoxy-substituted benzazirine (Figure X.46).

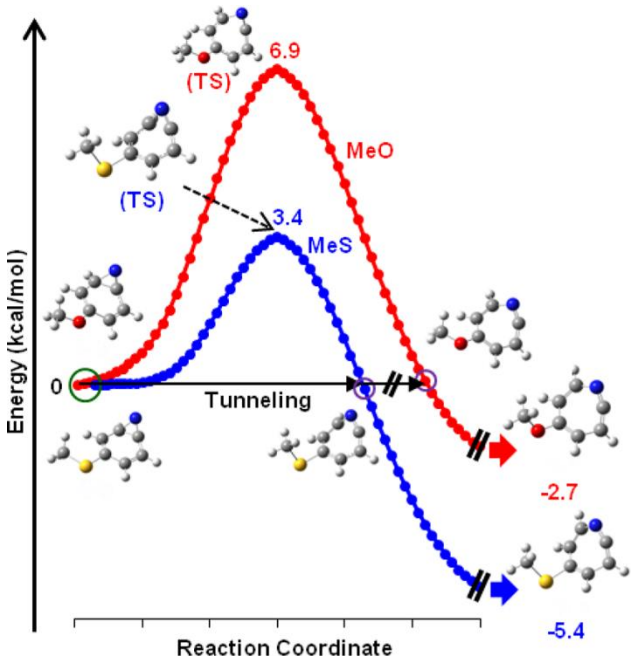

Figure X.46. B3LYP/6-31G(d) computed intrinsic reaction path for the transformation of benzazirine **39** to ketenimine **40** (blue) and the corresponding methoxy substituted derivative (red). Adapted from Ref. 172 with permission from the American Chemical Society. Copyright 2013.

In our study,[173] we showed that benzazirine **41**, generated *in situ* upon 530 nm irradiation of protium and deuterated triplet 2−formylphenylnitrene, spontaneously undergoes ring-expansion to ketenimine **42** under cryogenic conditions (see Figure X.45). In an argon matrix at 10 K and under dark, ~25% of **41**-d rearranges to **42**-d after 5 days. Using IR spectroscopy, we determined a rate constant of $\sim 7.4 \times 10^{-7}$ s^{-1} (a half-life time of ~260 h) for this process. Upon increasing the absolute temperature the reaction rate hardly show any increase ($\sim 8.9 \times 10^{-7}$ s^{-1} at 20 K), which provides a strong evidence for the occurrence of heavy-atom tunneling.

Computed rate constants without and with tunneling consideration [using canonical variational transition state theory (CVT) and small curvature tunneling (SCT), respectively], confirm that the observed process can only take place by tunneling from the ground state (Figure X.47).[173] The estimated CVT rate constant at 10 K was 1.8×10^{-177} s^{-1}, which indicates that the thermal reaction is impossible to occur, whereas the estimated SCT rate constant was 3.5×10^{-5} s^{-1} (half-life time of ~6 h), which is comparable to the experimental result. The difference (computed around 40 times faster) is justifiable considering errors resulting from the used DFT/M06-2X computations [*e.g.*, M06-2X gives an energy barrier of 30 kJ mol^{-1} for the ring-expansion of **41** to **42**, which is about 5 kJ mol^{-1} lower than that calculated at the more precise CCSD(T) level]. A small secondary kinetic isotopic effect, resulting in the acceleration of the reaction upon substitution of deuterium by protium in the formyl group of benzazirine **41**, was also predicted theoretically and measured experimentally. Very interestingly, it was also observed that the reaction rate for the ring-expansion of **41** to **42** is one order of magnitude larger (faster) when the sample at 10 K is exposed to the radiation of the spectrometer IR globar source. This

suggests the possibility of occurrence of IR-induced photochemistry, or IR-assisted tunneling.

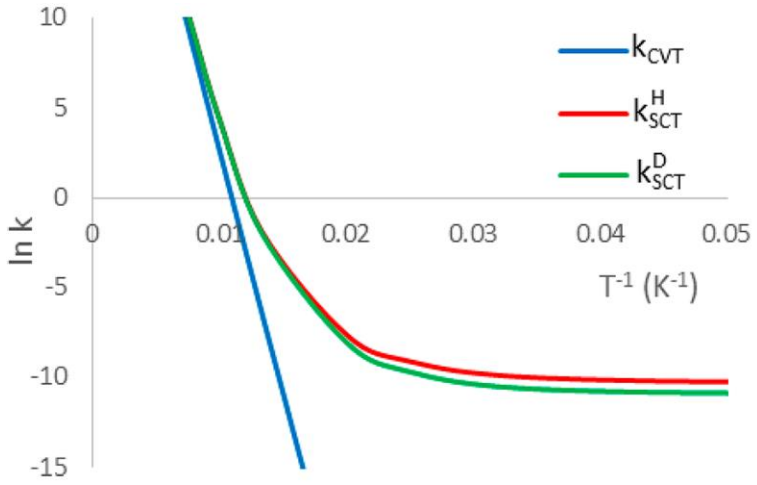

Figure X.47. Arrhenius graph for the ring-expansion of benzazirine **41** to cyclic ketenimine **42** reaction without (CVT) and with (SCT) tunneling corrections, computed at the M06-2X/6-311+G(2d,p) level. Adapted from Ref. 173 with permission from the American Chemical Society. Copyright 2017.

Direct spectroscopic evidence of heavy-atom tunneling under low temperature matrix isolation conditions was also reported for cases involving singlet carbene species (Figure X.48).[174-175] Zuev and Sheridan found that upon irradiation (334 nm) of *tert*-butylchlorodiazirine in a N_2 matrix at 11 K, the IR bands associated with the photogenerated carbene **43** slowly disappeared, while the IR bands of cyclopropane **44** simultaneously increased.[174] The rate constant for the decay of **43** varied from 4×10^{-4} s^{-1}, initially, to 3×10^{-5} s^{-1}, at one-half of the conversion (a typical dispersive kinetics behavior). The rate of the reaction was observed to be insensitive to temperature on warming the matrix from 11 to 30 K, which signals the existence of tunneling. Interestingly, it was found that perdeuterated carbene **43** was stable under the matrix isolation conditions. This extremely large kinetic isotope effect reflects the

expected significant role that the H-atom movement plays in the tunneling reaction. Nonetheless, the 1,3-CH insertion reaction of carbene **43** implies formation of a C-C bond during the process leading to **44** and that carbon-atom tunneling must also be involved.

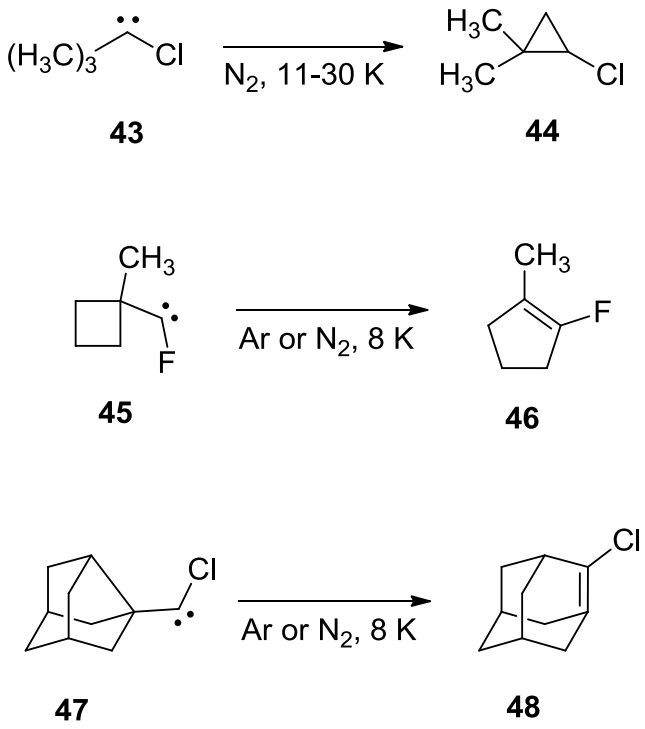

Figure X.48. Rearrangement reaction of carbenes **43**, **45** and **47** to species **44**, **46** and **48**, respectively.

Later, the same authors published another example of tunneling involving carbenes trapped in cryogenic matrices.[175] Fluorocarbene **45** and fluorocyclopentene **46** were generated in a nitrogen matrix at 8 K by irradiation of a diazo precursor with visible light (>550 nm). Subsequent irradiation at 436 nm caused rapid disappearance of the IR bands of carbene **45** and simultaneous growth of those of cyclopentene **46**. Even under exclusion of light, a slow rearrangement of **45** to **46** was observed at 8 K. In an N_2 matrix at 8 K under dark, the most reactive conformer of **45** was observed to

decay following a first order kinetics, in the first 20% of conversion, with a rate constant of 4×10^{-6} s^{-1}. In an Ar matrix at 8 K, carbene **45** was found to undergo ring expansion with a rate one order of magnitude faster, *ca.* 4×10^{-5} s^{-1}. When the Ar matrix was warmed to 16 K, the ring expansion rate of **45** increases only by a factor of 2, to *ca.* 9×10^{-5} s^{-1} (in the N_2 matrix tripling the temperature accelerates the ring-expansion of **45** by a factor of about 100). These findings were interpreted as an indication that ring expansion of **45** occurs by carbon-atom tunneling.

To confirm that carbon-atom tunneling provides an explanation for the experimental results, tunneling reaction rates were calculated.[175] At the MPW1K/6-31+G(d,p) level, the ring-expansion of carbene **45** to cyclopentene **46** was computed to have a barrier of 27 kJ mol^{-1} and to be 328 kJ mol^{-1} exothermic. Arrhenius plots for the rate constants of the **45** → **46** transformation, calculated using the SCT approximation as well as the CVT theory, predict a rate constant of 9×10^{-6} s^{-1} at the low temperature limiting (T< 20 K) when tunneling is included and a classical rate constant 2×10^{152} times smaller. The reaction coordinate mode was calculated to have a frequency of 69 cm^{-1}, and therefore, at 8 K tunneling should occur almost exclusively from the $v = 0$ vibrational ground state. At 16 K, the fraction of reaction occurring out of the $v = 1$ vibrational level can be estimated to increase to 6%. Theory predicts that this will produce a negligible change in rate, so the observed increase in the rate constant upon the temperature increase was interpreted as due to environmental effects resulting from the matrix softening.

The last example reported here known of heavy-atom tunneling in a singlet carbene species involves the ring expansion of a noradamantylchlorocarbene. In a collaborative effort, Moss, Sauers, Sheridan and others[176] described the generation of carbene **47** upon irradiation (334 nm) of a diazirine precursor in an N_2 matrix at 8

K. Product **47** was characterized using IR and UV-vis spectroscopies with the support of B3LYP/6-31+G(d,p) computations. In the absence of light, matrix-isolated carbene **47** was found to slowly rearrange to **48**. Following the evolution of the IR spectra along the transformation, it was determined that 15% of **47** was converted into **48** after 3 days ($k \approx 2.3 \times 10^{-7}$ s^{-1}). The rearrangement rate of **47** was a bit faster (35% conversion over the same time) at 23 K. The experimentally observed behaviour was similar to that found for carbene **45** ring-expansion to **46**, which led the authors to propose that rearrangement of **47** to **48** also proceeds *via* heavy-atom tunneling.

B3LYP/6-31+G(d,p) computations predict a barrier of 22 kJ mol^{-1} for the **47** → **48** rearrangement, which precludes the possibility of classical over-the-barrier reaction at the used cryogenic temperatures. The lower exothermicity for the reaction of **47** comparing with that of **45** (86 *vs*. 328 kJ mol^{-1}) probably makes the width of the barrier larger and explains the slower tunneling rate for **47** → **48** in comparison with that for **45** → **46**, despite the smaller barrier height for the former transformation (22 *vs.* 27 kJ mol^{-1}).

The first case of heavy-atom tunneling involving a nitrene species was reported in 2017 by Zeng, Abe and co-workers (Figure X.49).[177] They generated triplet trifluoroacetyl nitrene ^{3}**49** by irradiating the corresponding azide precursor in solid matrices (Ar, Ne and N_2) with a 193 nm laser. Isocyanate **50** was the main product observed. The weak IR bands assigned to ^{3}**49** were found to vanish quickly even at 2.8 K and while keeping the matrix in the dark (Figure X.50). Concomitantly, the intensity of the IR bands of **50** increased. First-order kinetics for the ^{3}**49** → **50** rearrangement were studied in various matrices and at different temperatures. Noteworthy, temperature independent rate constants were observed in the 2.8−23.0

K range. For instance, rate constants of 11.9×10^{-4} and 12.8×10^{-4} s^{-1} (half-life time of < 10 min) were obtained in Ar matrices at 2.8 and 19.0 K, respectively. The fast and temperature independent rearrangement of nitrene ^{3}**49** at extremely low temperatures can only take place by a mechanism of heavy-atom tunneling. The unexpectedly observed large $^{14}N/^{15}N$ kinetic isotopic effect (1.18–1.33) indicates that the tunneling rearrangement does not occur solely by shift of the CF_3 fragment, but that the nitrogen atom also plays a significant role in the reaction.

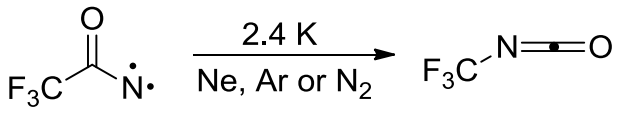

49 **50**

Figure X.49. Rearrangement reaction of triplet nitrene ^{3}**49** to isocyanate **50**.

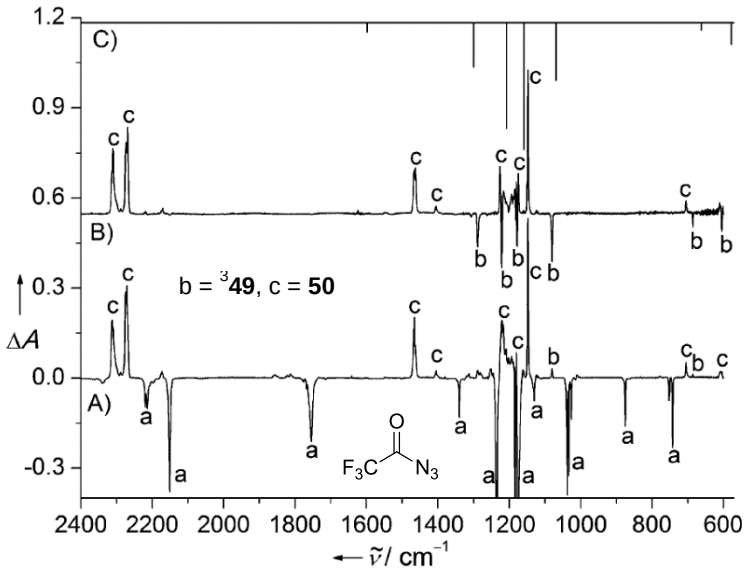

Figure X.50. (A): IR difference spectrum showing the change upon the 193 nm laser photolysis of azide precursor (a) in solid Ar at 2.8 K. (B): IR difference spectrum showing the conversion from triplet nitrene **49** (b) to singlet isocyanate **50** (c) after standing the sample in the dark for 60 min at 2.8 K. (C): Computed IR spectrum of ^{3}**49**. Reproduced from Ref. 177 with permission from John Wiley and Sons. Copyright 2017 Wiley-VCH Verlag GmbH & Co. KGaA, Weinheim.

As expected, calculations indicate that the triplet state of **49** is lower in energy than the singlet state (by 50 and 30 kJ mol^{-1}, at M06-2X/6-311+G(3df,3pd) and CASPT2(10,10)/6-311G** levels, respectively). One minimum energy crossing point (MECP) connecting the triplet **49** and the singlet **50** product was located 58.5 kJ mol^{-1} above ^{3}**49** [at the B3LYP/6-311+G(3df,3pd) level]. This estimated rearrangement barrier reinforces the conclusion that only tunneling can explain the observed reaction at cryogenic temperatures. In less inert organic matrices, like 2-methyltetrahydrofuran or toluene, the tunneling transformation was dramatically influenced (the kinetics was considerably reduced), implying that for this system intermolecular interactions can have a huge effect on the tunneling probability.

The most recent example (2019) of heavy-atom tunneling observed in cryogenic matrix conditions was reported by our group in collaboration with Schreiner's group (Figure X.51).[178] Triplet arylnitrene ^{3}**51** was first generated by photolysis (254 nm) of *p*-azidoaniline in an Ar matrix at 3 K and its vibrational signature was obtained. Subsequently, nitrene ^{3}**51** was depleted by irradiation at λ = 435 nm, resulting in the formation of the cyclic ketenimine **53** and a small amount of benzazirine **52**. Ketenimine **53** was selectively converted to nitrene ^{3}**51** by irradiation at λ = 350 nm, and a clear spectroscopic IR signature of these two species was obtained. In Ar at 3 K under the dark, benzazirine **52** was found to spontaneously decay, and surprisingly the rearrangement reaction simultaneously yielded two products, namely triplet nitrene ^{3}**51** and singlet ketenimine **53** (Figure X.52).

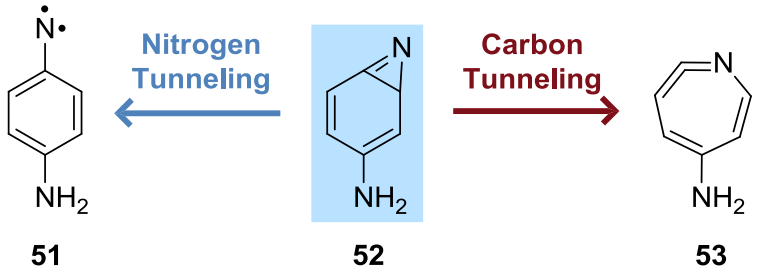

Figure X.51. Competitive ring-open *vs.* ring-expansion reaction of benzazirine **52** to triplet nitrene ^{3}**51** and cyclic ketenimine **53**, respectively.

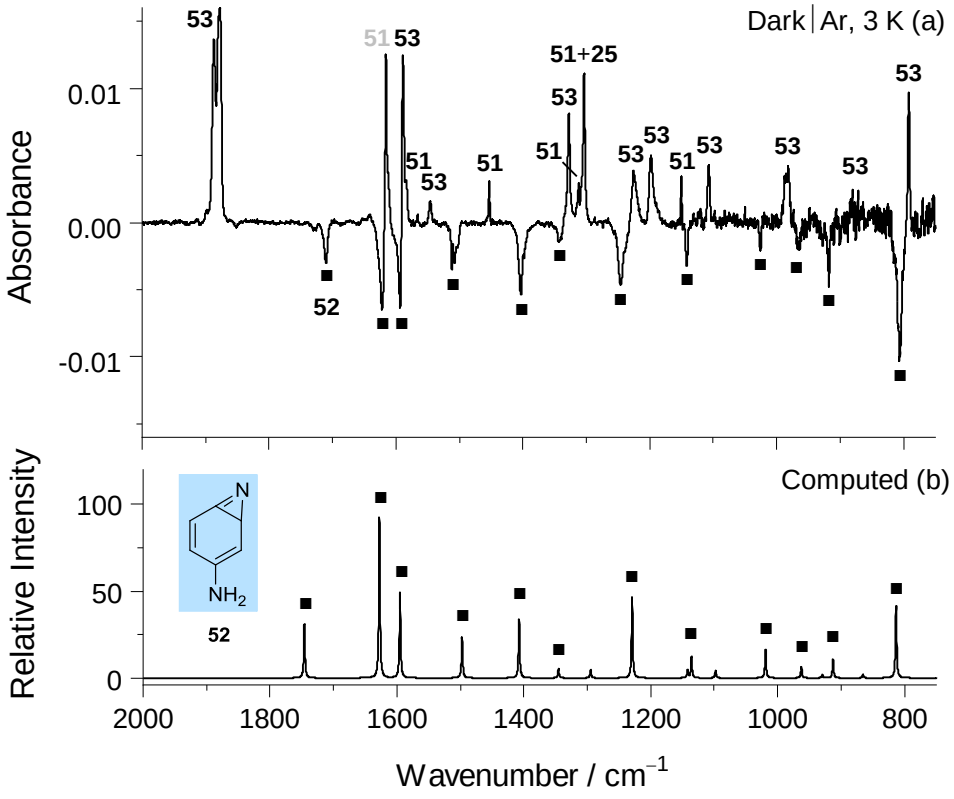

Figure X.52. (a) Experimental difference IR spectrum showing changes after keeping the sample at 3 K (argon matrix) in the dark for 24 h, subsequent to depletion of nitrene ^{3}**51** at λ = 435 nm. The downward bands are due to the consumption of benzazirine **52**. The upward bands are due to the formation of both ^{3}**51** and **53**. (b) IR spectrum of **52** computed at B3LYP/6-311+G(2d,p) level of theory. Adapted from Ref. 178 with permission from the American Chemical Society. Copyright 2019.

A detailed assignment of the IR spectrum of **52** was performed with the support of the B3LYP/6-311+G(2d,p) computed IR spectrum. Under these conditions, a rate constant of ~5.5 × 10^{-5} s^{-1} was obtained (half-life time of ~210 min) and the product ^{3}**51**:**53** ratio was found to be roughly 15:85. Kinetic measurements were also performed at 10 and 18 K, and resulted in rate constants of ~6.0 × 10^{-5} and ~7.0 × 10^{-5} s^{-1}, respectively, *i.e.*, the rearrangement rate of **52** barely shows an increase upon increasing the absolute temperature by a factor up to five. Moreover, the product ^{3}**51**:**53** ratio practically did not change with the increase of temperature (18:82 at 10 K and 17:83 at 18 K). Therefore, it became evident that the rearrangements of **52** in cryogenic conditions, leading to the formation of ^{3}**51** and **53** were not due to thermally activated processes but to two independent and competitive heavy-atom tunneling reactions.

The formation of ^{3}**51** conceivably involves the ring-opening of **52** to open-shell singlet (OSS) **51** followed by fast ISC. Because OSS **51** can only be adequately described using a multi-configurational wave function, the ring-opening **52** → OSS **51** was computed at the NEVPT2(8,8) level, and an energy barrier of 10 kJ mol^{-1} was obtained. For the ring-expansion **52** → **53**, computations at the CCSD(T) level were found more reliable, and an energy barrier of 30 kJ mol^{-1} was obtained. Even a smaller barrier of ~10 kJ mol^{-1} is prohibitive at the cryogenic temperatures of the experiment, and according to the classic rate theory, **52** should be stable (a half-life time of ~10^{162} years at 3 K is predicted). In addition, the observed major product **53** is separated by a higher computed energy barrier than the minor product ^{3}**51**. This contradicts the rules inferred from classical TST and can only be explained considering the occurrence of heavy-atom tunneling reactions and tunneling control of the global chemical reactivity exhibited by benzazirine **52**.[19]

Computed tunneling half-lives using the one-dimensional WKB formalism do indeed predict the existence of two competitive tunneling reactions from **52**, in accordance with the experimental observations.[178] Moreover, computations also showed that in the ring-opening **52** → OSS **51**, the nitrogen atom in the three-membered ring is the heavy atom having by far the largest displacement (a traversed arc of ~0.56 Å), making the case for a predominant nitrogen atom tunneling. Regarding the ring-expansion **52** → **53**, the two carbon atoms in the three-membered ring are clearly the heavy atoms with the largest displacements (a traversed arc of ~0.32 Å each), making the case for a predominant carbon atom tunneling. With this discovery, we unveiled a new reactivity paradigm in this area, by demonstrating that a well-defined chemical starting material decays spontaneously at cryogenic temperature into two different products that arise from competitive heavy-atom carbon *vs.* nitrogen tunneling reactions.

Author Contributions

C. M. N. wrote the first version of sections X.1 and X.8; I. R. wrote the first version of sections X.2, X.4, X.5, and X.7; R. F. wrote the first version of sections X.3 and X.6. All authors contributed to the preparation of the final version of all sections.

Acknowledgements

This work was supported by Projects POCI-01-0145-FEDER-028973 and POCI-01-0145-FEDER-016617 (PTDC/QEQ-QFI/3284/2014), funded by FEDER, *via* Portugal 2020-POCI, by National Funds *via* the Portuguese Foundation for Science and

Technology (FCT), by bilateral project for scientific cooperation between FCT (Portugal) and DAAD (Germany), and by bilateral project for scientific cooperation between FCT (Portugal) and PHC Pessoa (France). The Coimbra Chemistry Centre is supported by the FCT through the project UID/QUI/0313/2019, cofunded by COMPETE. C.M.N. and I.R. acknowledge the FCT for an Auxiliary Researcher grant and an Investigador FCT grant, respectively.

References

1 F. Hund, *Z. Phys.*, 1927, **43**, 805–826.

2 E. P. Wigner, *Z. Phys. Chem.*, 1932, **19B**, 203–216.

3 R. P. Bell, *Proc. R. Soc. A Math. Phys. Eng. Sci.*, 1933, **139**, 466–474.

4 S. Roginsky and L. Rosenkewitsch, *Nature*, 1930, **125**, 347–348.

5 D. G. Bourgin, *Proc. Natl. Acad. Sci.*, 1929, **15**, 357–362.

6 R. P. Bell, *The Tunnel Effect in Chemistry*, Springer, Boston, MA, 1980.

7 Form more recent books addressing tunneling effects in chemistry see: (a) H. Nakamura, G. Mil'nikov *Quantum Mechanical Tunneling in Chemical* Physics, CRC Press, 2013; (b) *Quantum Tunnelling in Enzyme-Catalysed Reactions*, Eds. R. K. Allemann, N. S. Scrutton, RSC, Cambridge, 2009; (c) At*om Tunneling Phenomena in Physics, Chemistry and Biology*, Eds. T. Miyazaki, Springer, Berlin, 2004.

8 P. Ball, *Beyond Weird: Why Everything You Thought You Knew About Quantum Physics Is Different*, University of Chicago Press, Chicago, 2018, ch.

3, pp. 38-57.

9 H. Eyring, *J. Chem. Phys.*, 1935, **3**, 107–115.

10 K. J. Laidler and C. King, *J. Phys. Chem.*, 1983, **87**, 2657–2664.

11 D. A. Dougherty and V. A. Eric, *Modern Physical Organic Chemistry*, University Science Books, Sausalito, CA, 2006.

12 S. Arrhenius, *Zeitschrift für Phys. Chemie*, 1889, **4**, 226–248.

13 E. F. Caldin, *Chem. Rev.*, 1969, **69**, 135–156.

14 R. S. Sheridan, in *Reviews of Reactive Intermediate Chemistry*, Wiley-Blackwell, 2006, pp. 415–463.

15 D. Ley, D. Gerbig and P. R. Schreiner, *Org. Biomol. Chem.*, 2012, **10**, 3781–3790.

16 E. M. Greer, K. Kwon, A. Greer and C. Doubleday, *Tetrahedron*, 2016, **72**, 7357–7373.

17 J. Meisner, J. Kästner, *Angew. Chem.-Int. Edit.*, 2016, **55**, 5400–5413.

18 J. Kästner, *WIREs Comput. Mol. Sci.*, 2014, **4**, 158–168.

19 P. R. Schreiner, *J. Am. Chem. Soc.*, 2017, **139**, 15276–15283.

20 R. J. Le Roy, H. Murai and F. Williams, *J. Am. Chem. Soc.*, 1980, **102**, 2325–2334.

21 D. G. Truhlar, *J. Phys. Org. Chem.*, 2010, **23**, 660–676.

22 W. T. Borden, *Wiley Interdiscip. Rev.-Comput. Mol. Sci.*, 2016, **6**, 20–46.

23 G. Wentzel, *Z. Phys.*, 1926, **38**, 518–529.

24 H. A. Kramers, *Z. Phys.*, 1926, **39**, 828–840.

25 L. Brillouin, *C. R. Hebd. Seances Acad. Sci.*, 1926, **183**, 24–26.

26 H. Jeffreys, *Proc. London Math. Soc.*, 1925, **23**, 428–436.

27 M. J. Frisch, G. W. Trucks, H. B. Schlegel, G. E. Scuseria, M. A. Robb, J. R. Cheeseman, G. Scalmani, V. Barone, B. Mennucci, G. A. Petersson, H. Nakatsuji, M. Caricato, X. Li, H. P. Hratchian, A. F. Izmaylov, J. Bloino, G. Zheng, J. L. Sonnenberg, M. Hada, M. Ehara, K. Toyota, R. Fukuda, J. Hasegawa, M. Ishida, T. Nakajima, Y. Honda, O. Kitao, H. Nakai, T. Vreven, J. A. Montgomery, Jr., J. E. Peralta, F. Ogliaro, M. Bearpark, J. J. Heyd, E. Brothers, K. N. Kudin, V. N. Staroverov, T. Keith, R. Kobayashi, J. Normand, K. Raghavachari, A. Rendell, J. C. Burant, S. S. Iyengar, J. Tomasi, M. Cossi, N. Rega, J. M. Millam, M. Klene, J. E. Knox, J. B. Cross, V. Bakken, C. Adamo, J. Jaramillo, R. Gomperts, R. E. Stratmann, O. Yazyev, A. J. Austin, R. Cammi, C. Pomelli, J. W. Ochterski, R. L. Martin, K. Morokuma, V. G. Zakrzewski, G. A. Voth, P. Salvador, J. J. Dannenberg, S. Dapprich, A. D. Daniels, Ö. Farkas, J. B. Foresman, J. V. Ortiz, J. Cioslowski and D. J. Fox Gaussian 09, Revision D.01; Gaussian, Inc.: Wallingford, CT, 2013.

28 P. R. Schreiner, H. P. Reisenauer, D. Ley, D. Gerbig, C. H. Wu and W. D. Allen, *Science*, 2011, **332**, 1300–1303.

29 M. Tsuge and L. Khriachtchev, *J. Phys. Chem. A*, 2015, **119**, 2628–2635.

30 I. Reva, M. J. Nowak, L. Lapinski and R. Fausto, *J. Chem. Phys.*, 2012, **136**, 064511 (1-8).

31 R. A. Marcus and M. E. Coltrin, *J. Chem. Phys.*, 1977, **67**, 2609–2613.

32 D. G. Truhlar and A. Kuppermann, *J. Am. Chem. Soc.*, 1971, **93**, 1840–1851.

33 R. T. Skodje, D. G. Truhlar and B. C. Garrett, *J. Phys. Chem.*, 1981, **85**, 3019–3023.

34 E. Whittle, D. A. Dows and G. C. Pimentel, *J. Chem. Phys.*, 1954, **22**, 1943.

35 I. Norman and G. Porter, *Nature*, 1954, **174**, 508–509.

36 C. Y. Lin and A. Krantz, *J. Chem. Soc. Chem. Commun.*, 1972, 1111–1112.

37 O. L. Chapman, C. L. McIntosh and J. Pacansky, *J. Am. Chem. Soc.*, 1973, **95**, 244–246.

38 R. G. S. Pong and J. S. Shirk, *J. Am. Chem. Soc.*, 1973, **95**, 248–249.

39 B. Meyer, *Low Temperature Spectroscopy*, American Elsevier Publishers Company, New York, 1971.

40 *Chemistry and Physics of Matrix Isolated Species*, ed. L. Andrews and M. Moskovits, Elsevier, Amsterdam, 1989.

41 *Matrix Isolation Spectroscopy*, ed. A. Barnes, W. J. Orville-Thomas, R. Gaufrès and A. Müller, Springer, 1981.

42 I. R. Dunkin, *Matrix Isolation Techniques: A Practical Approach*, Oxford University Press, 1998.

43 *Low Temperature Molecular Spectroscopy*, ed. R. Fausto, NATO-ASI Series C483, Kluwer, Amsterdam, 1996.

44 R. Fausto, *Photogeneration of Rare Molecules in Cryogenic Matrices:*

Spectroscopists' Adventures in Wonderland, in *Frontiers and Advances in Molecular Spectroscopy*, Ed. J. Laane, Elsevier, Amsterdam, 2018, Chapter 19, pp. 631–666.

45 I. Reva, M. J. Nowak, L. Lapinski and R. Fausto, *J. Chem. Phys.*, 2012, **136**, 064511 (1-8).

46 A. Plonka, *Radiat. Phys. Chem.*, 1991, **37**, 411–415.

47 A. Plonka, W. Lefik and J. Kroh, *Chem. Phys. Lett.*, 1979, **62**, 271–274.

48 A. Plonka and A. Paszkiewicz, *J. Chem. Phys.*, 1992, **96**, 1128–1133.

49 A. Plonka and A. Paszkiewicz, *Chem. Phys.*, 1996, **212**, 1–8.

50 M. B. Sponsler, R. Jain, F. D. Coms and D. A. Dougherty, *J. Am. Chem. Soc.*, 1989, **111**, 2240–2252.

51 W. Siebrand and T. A. Wildman, *Accounts Chem. Res.*, 1986, **19**, 238–243.

52 A. Plonka, Annu. Rep. Prog. Chem., Sect. C: Phys. Chem., 1988, **85**, 47–75.

53 M. Ertelt, D. A. Hrovat, W. T. Borden and W. Sander, *Chem.-Eur. J.*, 2014, **20**, 4713–4720.

54 C. M. Nunes, S. N. Knezz, I. Reva, R. Fausto and R. J. McMahon, *J. Am. Chem. Soc.*, 2016, **138**, 15287–15290.

55 I. Reva, C. M. Nunes, M. Biczysko and R. Fausto, *J. Phys. Chem. A*, 2015, **119**, 2614–2627.

56 L. Lapinski, I. Reva, M. J. Nowak and R. Fausto, *Phys. Chem. Chem. Phys.*, 2011, **13**, 9676–9684.

57 L. Lapinski, M. J. Nowak, I. Reva, H. Rostkowska and R. Fausto, *Phys. Chem. Chem. Phys.*, 2010, **12**, 9615–9618.

58 L. Lapinski, I. Reva, H. Rostkowska, R. Fausto and M. J. Nowak, *J. Phys. Chem. B*, 2014, **118**, 2831–2841.

59 A. J. Lopes Jesus, C. M. Nunes, I. Reva, S. M. V. Pinto and R. Fausto, *J. Phys. Chem. A*, 2019, **123**, 4396–4405.

60 S. Góbi, C. M. Nunes, I. Reva, G. Tarczay and R. Fausto, *Phys. Chem. Chem. Phys.*, 2019, **21**, 17063–17071.

61 M. Pettersson, J. Lundell, L. Khriachtchev and M. Räsänen, *J. Am. Chem. Soc.*, 1997, **119**, 11715–11716.

62 M. Pettersson, E. M. S. Maçôas, L. Khriachtchev, J. Lundell, M. Räsänen and R. Fausto, *J. Chem. Phys.*, 2002, **117**, 9095–9098.

63 E. M. S. Maçôas, J. Lundell, M. Pettersson, L. Khriachtchev, R. Fausto and M. Räsänen, *J. Mol. Spectrosc.*, 2003, **219**, 70–80.

64 M. Pettersson, E. M. S. Maçôas, L. Kriachtchev, R. Fausto and M. Räsänen, *J. Am. Chem. Soc.*, 2003, **125**, 4058–4059.

65 L. Khriachtchev, E. M. S. Maçôas, M. Pettersson and M. Räsänen, *J. Am. Chem. Soc.*, 2002, **124**, 10994–10995.

66 A. J. Lopes Jesus, C. M. Nunes, R. Fausto and I. Reva, *Chem. Comm.*, 2018, **54**, 4778–4781.

67 B. Kovács, N. Kuş, G. Tarczay and R. Fausto, *J. Phys. Chem. A*, 2017, **121**, 3392–3400.

68 A. J. Lopes Jesus, I. Reva and R. Fausto, *J. Chem. Phys.*, 2016, **144**, 124306 (1–9).

69 C. M. Nunes, I. Reva and R. Fausto, *Phys. Chem. Chem. Phys.*, 2019, **21**. 24993-25001.

70 E. M. S. Maçôas, L. Khriachtchev, M. Pettersson, R. Fausto and M. Räsänen, *J. Am. Chem. Soc.*, 2003, **125**, 16188–16189.

71 E. M. S. Maçôas, L. Kriachtchev, R. Fausto and M. Räsänen, *J. Phys. Chem. A*, 2004, **108**, 3380–3389.

72 E. M. S. Maçôas, L. Kriachtchev, M. Pettersson, R. Fausto and M. Räsänen, *J. Chem. Phys.*, 2004, **121**, 1331–1338.

73 E. M. S. Maçôas, L. Khriachtchev, M. Pettersson, R. Fausto and M. Räsänen, *J. Phys. Chem. A*, 2005, **109**, 3617–3625.

74 R. F. G. Apóstolo, R. R. F. Bento, G. Tarczay and R. Fausto, *J. Mol. Struct.*, 2016, **1125**, 288–295.

75 R. F. G. Apóstolo, R. R. F. Bento and R. Fausto, *Croat. Chim. Acta*, 2015, **88**, 377–386.

76 R. F. G. Apóstolo, G. Bazsó, G. O. Ildiz, G. Tarczay and R. Fausto, *J. Chem. Phys.*, 2018, **148**, 044303 (1–12).

77 G. Bazsó, S. Góbi and G. Tarczay, *J. Phys. Chem. A*, 2012, **116**, 4823–4832.

78 S. Lopes, T. Nikitin and R. Fausto, *J. Chem. Phys.*, 2019, **123**, 1581–1593.

79 N. Kuş and R. Fausto, *J. Chem. Phys.*, 2014, **141**, 234310 (1–14).

80 I. D. Reva, S. Stepanian, L. Adamowicz and R. Fausto, *J. Phys. Chem. A*,

2001, **105**, 4773–4780.

81 I. D. Reva, S. Jarmelo, L. Lapinski and R. Fausto, *J. Phys. Chem. A*, 2004, **108**, 6982–6989.

82 A. Halasa, L. Lapinski, I. Reva, H. Rostkowska, R. Fausto and M. J. Nowak, *J. Phys. Chem. A*, 2014, **118**, 5626–5635.

83 D. Gerbig and P. R. Schreiner, *J. Phys. Chem. B*, 2015, **11**, 693–703.

84 N. Kuş and R. Fausto, *J. Chem. Phys.*, 2017, **146**, 124305 (1–13).

85 L. Lapinski, I. Reva, H. Rostkowska, R. Fausto and M. J. Nowak, *J. Phys. Chem. A*, 2013, **117**, 5251–5259.

86 A. Halasa, L. Lapinski, I. Reva, H. Rostkowska, R. Fausto and M. J. Nowak, *J. Phys. Chem. A*, 2015, **119**, 1037–1047.

87 L. L. G. Justino, I. Reva and R. Fausto, *J. Chem. Phys.*, 2016, **145**, 014304 (1–13).

88 S. Amiri, H. P. Reisenauer and P. R. Schreiner, *J. Am. Chem. Soc.*, 2010, **132**, 15902–15904.

89 S. Nishino and M. Nakata, *J. Phys. Chem. A*, 2007, **111**, 7041–7047.

90 E. M. S. Maçôas, R. Fausto, M. Pettersson, L. Khriachtchev and M. Räsänen, *J. Phys. Chem. A*, 2000, **104**, 6956–6961.

91 E. M. S. Maçôas, R. Fausto, J. Lundell, M. Pettersson, L. Khriachtchev and M. Räsänen, *J. Phys. Chem. A*, 2000, **104**, 11725–11732.

92 E. M. S. Maçôas, R. Fausto, J. Lundell, M. Pettersson, L. Khriachtchev and M. Räsänen, *J. Phys. Chem. A*, 2001, **105**, 3922–3933.

93 A. Halasa, I. Reva, L. Lapinski, M. J. Nowak and R. Fausto, *J. Phys. Chem. A*, 2016, **120**, 2078–2088.

94 P. R. Schreiner, J. P. Wagner, H. P. Reisenauer, D. Gerbig, D. Ley, J. Sarka, A. G. Császár, A. Vaughn and W. D. Allen, *J. Am. Chem. Soc.*, 2015, **137**, 7828–7834.

95 N. Kuş, A. Sharma, I. Peña, M. C. Bermúdez, C. Cabezas, J. L. Alonso and R. Fausto, *J. Chem. Phys.*, 2013, **138**, 144305 (1–10).

96 C. M. Nunes, L. Lapinski, R. Fausto and I. Reva, *J. Chem. Phys.*, 2013, **138**, 125101 (1–12).

97 G. Bazsó, G. Magyarfalvi and G. Tarczay, *J. Phys. Chem. A*, 2012, **116**, 10539–10547.

98 G. Bazsó, E. E. Najbauer, G. Magyarfalvi and G. Tarczay, *J. Phys. Chem. A*, 2013, **117**, 1952–1962.

99 G. Bazsó, G. Magyarfalvi and G. Tarczay, *J. Mol. Struct.*, 2012, **1025**, 33–42.

100 E. E. Najbauer, G. Bazsó, R. Apóstolo, R. Fausto, M. Biczysko, V. Barone and G. Tarczay, *J. Phys. Chem. B*, 2015, **119**, 10496–10510.

101 E. E. Najbauer, G. Bazsó, S. Góbi, G. Magyarfalvi and G. Tarczay, *J. Phys. Chem. B*, 2014, **118**, 2093–2103.

102 I. D. Reva, S. G. Stepanian, L. Adamowicz and R. Fausto, *Chem. Phys. Lett.*, 2003, **374**, 631–638.

103 I. D. Reva, A. J. Lopes Jesus, M. T. S. Rosado, R. Fausto, M. E. Eusébio and J. S. Redinha, *Phys. Chem. Chem. Phys.*, 2006, **8**, 5339–5349.

104 S. Lopes, A. V. Domanskaya, R. Fausto, M. Räsänen and L. Khriachtchev, *J. Chem. Phys.*, 2010, **133**, 144507 (1–7).

105 S. Lopes, A. Domanskaya, M. Räsänen, L. Khriachtchev and R. Fausto, *J. Chem. Phys.*, 2015, **143**, 104307 (1–18).

106 J. Lundell, M. Räsänen and Z. Latajka, *Chem. Phys.*, 1994, **189**, 245–260.

107 P. K. Wawrzyniak, J. Panek, J. Lundell and Z. Latajka, *J. Mol. Model.*, 2005, **11**, 351–361.

108 P. K. Wawrzyniak, J. Panek, Z. Latajka and J. Lundell, *J. Mol. Struct.*, 2004, **704**, 297–304.

109 L. Khriachtchev, *J. Mol. Struct.*, 2008, **880**, 14–22.

110 A. Domanskaya, K. Marushkevich, L. Khriachtchev and M. Räsänen, *J. Chem. Phys.*, 2009, **130**, 154509 (1–5).

111 K. Marushkevich, L. Khriachtchev and M. Räsänen, *J. Chem. Phys.*, 2007, **126**, 241102 (1–4).

112 K. Marushkevich, M. Siltanen, M. Räsänen, L. Halonen and L. Khriachtchev, *J. Phys. Chem. Lett.*, 2011, **2**, 695–699.

113 L. Khriachtchev, A. Domanskaya, K. Marushkevich, M. Räsänen, B. Grigorenko, A. Ermilov, N. Andrijchenko and A. Nemukhin, *J. Phys. Chem. A*, 2009, **113**, 8143–8146.

114 K. Marushkevich, L. Khriachtchev and M. Räsänen, *J. Phys. Chem. A*, 2007, **111**, 2040–2042.

115 S. Lopes, R. Fausto and L. Khriachtchev, *J. Chem. Phys*., 2016, **144**, 084308

(1–11).

116 M. J. Nowak, I. Reva, A. J. Lopes Jesus, L. Lapinski and R. Fausto, *Phys. Chem. Chem. Phys.*, 2019, **21**, 22857-22868.

117 S. Nanbu, M. Sekine, M. Nakata, *J. Mol. Struct.*, 2012, **1025**, 69–73.

118 S. Nanbu, M. Sekine, M. Nakata, *J. Phys. Chem. A.*, 2011, **115**, 9911–9918.

119 N. Akai, S. Kudoh and M. Nakata, *J. Phys. Chem. A.*, 2003, **107**, 3655–3659.

120 N. Akai, S. Kudoh, M. Takayanagi and M. Nakata, *J. Phys. Chem. A.*, 2002, **106**, 11029–11033.

121 N. Akai, S. Kudoh, M. Takayanagi and M. Nakata, *Chem. Phys. Lett.*, 2002, **356**, 133–139.

122 M. M. Linden, J. P. Wagner, B. Bernhardt, M. A. Bartlett, W. D. Allen and P. R. Schreiner, *J. Chem. Phys. Lett.*, 2018, **9**, 1663–1667.

123 R. L. Redington, *J. Chem. Phys.*, 2000, **113**, 2319–2335.

124 A. S. Trivella, S. Coussan, T. Chiavassa, P. Theulé, P. Roubin and C. Manca, *Low Temp. Phys.*, 2006, **32**, 1042–1049.

125 N. O. B. Lüttschwager, T. N. Wassermann, S. Coussan and M. A. Suhm, *Mol. Phys.*, 2013, **111**, 2211–2227.

126 F. Wu, Y. H. Ren and W. S. Bian, *J. Chem. Phys.*, 2016, **145**, 074309 (1–9).

127 A. Gutiérrez-Quintanilla, M. Chevalier and C. Crépin, *Phys. Chem. Chem. Phys.*, 2016, **18**, 20713–20725.

128 H. Tomioka, *Res. Chem. Intermed.*, 1994, **20**, 605–634.

129 C. Wentrup, *Angew. Chem.-Int. Edit.*, 2018, **57**, 11508–11521.

130 O. L. Chapman, *Pure Appl. Chem.*, 1979, **51**, 331–339.

131 M. S. Platz, *J. Am. Chem. Soc.*, 1979, **101**, 3398–3399.

132 R. J. McMahon and O. L. Chapman, *J. Am. Chem. Soc.*, 1987, **109**, 683–692.

133 M. S. Platz, *J. Am. Chem. Soc.*, 1980, **102**, 1192–1194.

134 M. S. Platz and J. R. Burns, *J. Am. Chem. Soc.*, 1979, **101**, 4425–4426.

135 M. C. Biewer, M. S. Platz, M. Roth and J. Wirz, *J. Am. Chem. Soc.*, 1991, **113**, 8069–8073.

136 C. R. Kemnitz, CW. L. Karney and W. T. Borden, *J. Am. Chem. Soc.*, 1998, **120**, 3499–3503.

137 A. Admasu, A. D. Gudmundsdottir and M. S. Platz, *J. Phys. Chem. A*, 1997, **101**, 3832–3840.

138 W. T. Borden, N. P. Gritsan, C. M. Hadad, W. L. Karney, C. R. Kemnitz and M. S. Platz, *Accounts Chem. Res.*, 2000, **33**, 765–771.

139 J. J. Fisher and J. Michl, *J. Am. Chem. Soc.*, 1987, **109**, 583–584.

140 J. C. Koziar and D. O. Cowan, *Accounts Chem. Res.*, 1978, **11**, 334–341.

141 P. R. Schreiner, H. P. Reisenauer, F. C. Pickard IV, A. C. Simmonett, W. D. Allen, E. Mátyus and A. G. Császár, *Nature*, 2008, **453**, 906–909.

142 D. Ley, D. Gerbig and P. R. Schreiner, *Chem. Sci.*, 2013, **4**, 677–684.

143 D. Gerbig, H. P. Reisenauer, C. H. Wu, D. Ley, W. D. Allen and P. R.

Schreiner, *J. Am. Chem. Soc.*, 2010, **132**, 7273–7275.

144 D. Ley, D. Gerbig, J. P. Wagner, H. P. Reisenauer and P. R. Schreiner, *J. Am. Chem. Soc.*, 2011, **133**, 13614–13621.

145 A. Mardyukov, H. Quanz and P. R. Schreiner, *Nat. Chem.*, 2017, **9**, 71–76.

146 P. R. Schreiner and H. P. Reisenauer, *Angew. Chem.-Int. Edit.*, 2008, **47**, 7071–7074.

147 A. Nandi, D. Gerbig, P. R. Schreiner, W. T. Borden and S. Kozuch, *J. Am. Chem. Soc.*, 2017, **139**, 9097–9099.

148 A. K. Eckhardt, D. Gerbig and P. R. Schreiner, *J. Phys. Chem. A*, 2018, **122**, 1488–1495.

149 A. K. Eckhardt, F. R. Erb and P. R. Schreiner, *Chem. Sci.*, 2019, **10**, 802–808.

150 J. Sarka, A. G. Császár and P. R. Schreiner, *Collect. Czech. Chem. Commun.*, 2011, **76**, 645–667.

151 H. Rostkowska, L. Lapinski, A. Khvorostov and M. J. Nowak, *J. Phys. Chem. A*, 2003, **107**, 6373–6380.

152 H. Rostkowska, L. Lapinski and M. J. Nowak, *Phys. Chem. Chem. Phys.*, 2018, **20**, 13994–14002.

153 H. Rostkowska, L. Lapinski, A. Khvorostov and M. J. Nowak, *Chem. Phys.*, 2004, **298**, 223–232.

154 L. Lapinski, H. Rostkowska, A. Khvorostov and M. J. Nowak, *Phys. Chem. Chem. Phys.*, 2003, **5**, 1524–1529.

155 B. B. Wright, V. P. Senthilnathan, M. S. Platz and C. W. McCurdy Jr., *Tetrahedron Lett.*, 1982, **23**, 833–836.

156 E. Mendez-Vega, M. Maehara, A. H. Raut, J. Mieres-Perez, M. Tsuge, Y. P. Lee and W. Sander, *Chem.-Eur. J.*, 2018, **24**, 18801–18808.

157 S. Henkel, M. Ertelt and W. Sander, *Chem.-Eur. J.*, 2014, **20**, 7585–7588.

158 P. S. Zuev and R. S. Sheridan, *J. Am. Chem. Soc.*, 2001, **123**, 12434–12435.

159 S. Henkel, Y. A. Huynh, P. Neuhaus, M. Winkler and W. Sander, *J. Am. Chem. Soc.*, 2012, **134**, 13204–13207.

160 S. Henkel and W. Sander, *Angew. Chem.-Int. Edit.*, 2015, **54**, 4603–4607.

161 I. Trosien, E. Mendez-Vega, T. Thomanek and W. Sander, *Angew. Chem.-Int. Edit.*, 2019, **58**, 14855–14859.

162 K. A. Haupa, G. Tarczay and Y.-P. Lee, *J. Am. Chem. Soc.*, 2019, **141**, 11614–11620.

163 S. Kozuch, A. Nandi and A. Sucher, *Chem. - A Eur. J.*, 2018, **24**, 16348–16355.

164 S. L. Buchwalter and G. L. Closs, *J. Am. Chem. Soc.*, 1975, **97**, 3875–3878.

165 S. L. Buchwalter and G. L. Closs, *J. Am. Chem. Soc.*, 1979, **101**, 4688–4694.

166 D. W. Whitman and B. K. Carpenter, *J. Am. Chem. Soc.*, 1982, **104**, 6473–6474.

167 B. K. Carpenter, *J. Am. Chem. Soc.*, 1983, **105**, 1700–1701.

168 A. M. Orendt, B. R. Arnold, J. G. Radziszewski, J. C. Facelli, K. D. Malsch, H.

Strub, D. M. Grant and J. Michl, *J. Am. Chem. Soc.*, 1988, **110**, 2648–2650.

169 T. Schleif, J. Mierez-Perez, S. Henkel, M. Ertelt, W. T. Borden and W. Sander, *Angew. Chemie Int. Ed.*, 2017, **56**, 10746–10749.

170 X. Zhang, D. A Hrovat and W. T. Borden, *Org. Lett.*, 2010, **12**, 2798–2801.

171 W. Sander, W. Müller and R. Sustmann, *Angew. Chemie - Int. Ed.*, 1988, **27**, 572–574.

172 H. Inui, K. Sawada, S. Oishi, K. Ushida and R. J. McMahon, *J. Am. Chem. Soc.*, 2013, **135**, 10246–10249.

173 C. M. Nunes, I. Reva, S. Kozuch, R. J. McMahon and R. Fausto, *J. Am. Chem. Soc.*, 2017, **139**, 17649–17659.

174 P. Zuev and R. D. Sheridan, *J. Am. Chem. Soc.*, 1994, 4123–4124.

175 P. S. Zuev, R. S. Sheridan, T. V Albu, D. G. Truhlar, D. A. Hrovat and W. T. Borden, *Science*, 2003, **299**, 867–870.

176 R. A. Moss, R. R. Sauers, R. S. Sheridan, J. Tian and P. S. Zuev, *J. Am. Chem. Soc.*, 2004, **126**, 10196–10197.

177 Z. Wu, R. Feng, H. Li, J. Xu, G. Deng, M. Abe, D. Bégué, K. Liu and X. Zeng, *Angew. Chem. Int. Ed.*, 2017, **56**, 15672–15676.

178 C. M. Nunes, A. K. Eckhardt, I. Reva, R. Fausto and P. R. Schreiner, *J. Am. Chem. Soc.*, 2019, **141**, 14340–14348.